

Effects of Linear Redshift Space Distortions and Perturbation Theory on BAOs: A 3D Spherical Analysis

Geraint Pratten¹ and Dipak Munshi^{1,2}

¹*School of Physics and Astronomy, Cardiff University, Queen's, Buildings, 5 The Parade, Cardiff, CF24 3AA, UK*

²*Department of Physics & Astronomy, University of Sussex, Brighton, BN1 9QH, UK*

31 August 2021, Revision: 0.9

ABSTRACT

The Baryon Acoustic Oscillations (BAO) are features in the matter power spectrum on scales of order $100 - 150 h^{-1}\text{Mpc}$ that promise to be a powerful tool to constrain and test cosmological models. The BAO have attracted such attention that future upcoming surveys have been designed with the BAO at the forefront of the primary science goals. Recent studies have advocated the use of a spherical-Fourier Bessel (sFB) expansion for future wide field surveys that cover both wide and deep regions of the sky necessitating the simultaneous treatment of the spherical sky geometry as well as the extended radial coverage. Ignoring the possible effects of growth, which is not expected to be significant at low redshifts, we present an extended analysis of the BAO's using the sFB formalism by taking into account the role of non-linearities and linear redshift distortions in the oscillations observed in the galaxy power spectrum. The sFB power spectrum has both radial and tangential dependence and it has been shown that in the limit that we approach a deep survey the sFB power spectrum is purely radial and collapses to the Cartesian Fourier power spectrum. This radialisation of information is shown to hold even in the presence of redshift space distortions (RSD) and 1-loop corrections to the galaxy power spectrum albeit with modified tangential and radial dependence. As per previous studies we find that the introduction of non-linearities leads to a damping of the oscillations in the matter power spectrum.

Key words: : Cosmology– Cosmic Microwave Background Radiation- Large-Scale Structure of Universe – Methods: analytical, statistical, numerical

1 INTRODUCTION

Observations of the cosmic microwave background (CMB) and large-scale structure (LSS) will carry complementary cosmological information. While all-sky CMB observations, such as NASA's WMAP¹ or ESA's Planck² experiments, primarily probe the distribution of matter and radiation at redshift $z = 1300$, large scale surveys such as ESA's Euclid³ or the Square Kilometer Array (SKA)⁴ will provide a window at lower redshifts on order $z \approx 0 - 2$. The study of

large scale structure appears to be a promising candidate in the study of the influence and role of the dark sectors in the standard model of cosmology. One particular phenomena of interest are the Baryon Acoustic Oscillations (BAOs) that manifest themselves in the matter power spectrum of galaxy clusters on cosmological scales of order $100h^{-1}\text{Mpc}$. These oscillations in the matter power spectrum are generated just before recombination through the interplay between a coupled photon-baryon fluid and gravitationally interacting dark matter (Sunyaev and Zeldovich 1970; Peebles and Yu 1970; Eisenstein et al 2005; Seo and Eisenstein 2003, 2007).

The scale of the peaks and oscillatory features of the BAOs promises to be an important cosmological tool that acts as a standard ruler from which we can investigate and constrain dark energy parameters (see Eisenstein et al (2005); Amendola, Quercellini and Gi-

¹ <http://map.gsfc.nasa.gov/>

² <http://sci.esa.int/planck>

³ <http://sci.esa.int/euclid>

⁴ <http://www.skatelescope.org/>

allongo (2005); Dolney, Jain and Takada (2006); Wang and Mukherjee (2006) for a small selection or representative literature), neutrino masses (Goobar, Hannestad, Mörtzell and Tu 2006), modified theories of gravitation (Alam and Sahni 2006; Lazkoz, Maartens and Majerotto 2006) and deviations from the standard model of cosmology (Garcia-Bellido and Haugboelle 2008, 2009; February, Clarkson and Maartens 2012)). Significant attention has been devoted to the BAOs and they were first detected with SDSS⁵ data (Eisenstein et al 2005; Adelman-McCarthy et al 2008) and in subsequent surveys (Colless et al 2003; Percival et al 2007).

The BAOs have been studied using standard Fourier space decompositions (Seo and Eisenstein 2003, 2007), real space analysis (Eisenstein et al 2005; Slosar, Ho, White and Louis 2009; Xu et al 2010; Juszkiewicz, Hellwing and van de Weygaert 2012), in 2D spherical harmonics defined on thin spherical shells (Dolney, Jain and Takada 2006), but also in the sFB expansion (Rassat and Refregier 2012). It is important to note that different frameworks will make use of different information and will therefore have different constraining power for different cosmological parameters emphasising the complementarity of mixed studies (Rassat et al 2008). Previous studies, having predominantly focused on projected 2D surveys, have discarded radial information by projecting galaxy positions into tomographic redshift bins however, such a loss of information could be avoided by adopting a full 3D description (e.g. Asorey et al (2012)).

Upcoming large scale structure surveys will provide cover for both large and deep areas of the sky and this will necessitate a formalism that can provide a simultaneous treatment of both the spherical sky geometry as well as an extended radial coverage. A natural basis for such a survey is provided by the sFB decomposition, (see Heavens and Taylor (1995); Fisher et al (1995); Percival et al (2004); Castro, Heavens and Kitching (2005); Erdogdu et al (2006); Abramo, Reimberg and Xavier (2010); Leistedt et al (2011); Shapiro, Crittenden and Percival (2011); Rassat and Refregier (2012); Lanusse, Rassat and Starck (2012); Asorey et al (2012) for an incomplete selection of literature on the subject). In this prescription we expand a 3D tracer field, such as the galaxy density contrast, using the radial (k) and tangential (i.e. along the surface of a sphere) (ℓ) dependence.

The galaxy matter power spectrum is conventionally modelled using cosmological perturbation theory (PT). The linear order results will be valid at large scales where non-linear growth of structure under gravitational instability can be neglected. At smaller scales it is no longer possible to neglect the non-linear growth of structure and we need to incorporate higher-order corrections to the matter power spectrum. There are a number of different approaches currently in the literature to tackle this problem and we will present a more detailed description later on. Non-linear galaxy clustering bias arises from a non-linear mapping between the underlying matter density field and observed collapsed objects (e.g. galaxies or dark matter haloes) and galaxy bias is, in essence, an isocurvature perturbation. Current literature has investigated more detailed prescriptions for galaxy bias such as the effects of primordial non-Gaussianity, scale dependence or non-local bias. Another form of non-linearity arises from RSD generated through the internal motion of galaxies within haloes. This ef-

fect is known as the Finger-of-God effect (Jackson 1972) and is distinct from the linear RSD considered in this paper (Kaiser 1987). It is also possible to investigate the role of non-Gaussian initial conditions, such as those generated in various inflationary models, and how this propagates non-linear corrections through to the growth of structure. The signatures of non-Gaussianity in these models will be distinctly different (e.g. a modified bispectrum) to the signatures of non-Gaussianity in models that have Gaussian initial conditions and are allowed to undergo gravitational collapse.

Throughout this paper we will follow the construction outlined in Rassat and Refregier (2012) and generalise the method to study the role of redshift space distortions (RSD) and the non-linear (NL) evolution of density perturbations. Previous investigations have used standard perturbation theory (SPT), galaxy bias models and Lagrangian perturbation theory (LPT) to characterise the role of various non-linear corrections to the BAO signal using the 3D Fourier power spectrum $P(k)$ (Jeong and Komatsu 2006; Nishimichi et al 2007; Jeong and Komatsu 2009; Nomura, Yamamoto and Nishimichi 2008; Nomura, Yamamoto, Huetsi and Nishimichi 2009). These non-linear corrections can be reassessed within the sFB framework to aid our understanding of how real world effects can impact the radialisation of information.

Recent work (Asorey et al 2012) utilising the sFB formalism has focused on how to recover the full 3D clustering information including RSD from 2D tomography using the angular auto and cross spectra of different redshift bins. Traditionally, RSD measurements have been made through spectroscopic redshift surveys such as the 2dF Galaxy Redshift Survey (Colless et al 2003) and the Sloan Digital Sky Survey (York et al 2000) with photometric surveys often being neglected because of the loss of RSD through photometric redshift errors. Upcoming surveys, spectroscopic and photometric, such as the Dark Energy Survey (DES)⁶, Euclid, SKA, Physics of the Accelerating Universe Survey (PAU)⁷ (Bentez et al 2009), Large Synoptic Survey Telescope (LSST)⁸ or the Panoramic Survey Telescope and Rapid Response System (PanStarrs)⁹ offer the possibility of investigating the BAO and RSD through angular or projected clustering measurements Bentez et al (2009); Nock, Percival and Ross (2010); Crocce, Fosalba, Castander and Gaztanaga (2010); Gaztanaga et al (2011); Laureijs et al (2011); Ross, Percival, Crocce, Cabr and Gaztanaga (2011).

As RSD and distortions arising from an incorrect assumption for the underlying geometry are similar (Alcock and Paczynski 1979) the analyses of RSD using 3D data has to be used in conjunction with geometrical constraints (Samushia et al 2011). As approaches based purely on angular correlation functions do not depend on the background cosmological model, the angular clustering measures will be considerably simpler. The sFB is something of a mid-point between these two approaches and will, in general, be sensitive to the choice of fiducial concordance cosmology. This paper is organised as follows. In §2 we discuss the sFB expansion. In §3 we outline the effect of lin-

⁵ <http://www.sdss.org/>

⁶ www.darkenergysurvey.org

⁷ www.pausurvey.org

⁸ www.lsst.org

⁹ pan-starrs.ifa.hawaii.edu

ear RSD and §4 is devoted to issues related to realistic surveys. In §5 we consider perturbative corrections to linear real-space results and consider the structure of the sFB spectra. Results are discussed in §6 and conclusions presented in §7. Discussions about finite size of the survey and discrete sFB transforms are detailed in the appendices.

Throughout we will adopt the WMAP 7 cosmological parameters (Komatsu et al 2011): $h = 0.7$, $\Omega_b h^2 = 0.0226$, $\Omega_c h^2 = 0.112$, $\Omega_\Lambda = 0.725$, $\sigma_8 = 0.816$.

2 SPHERICAL FOURIER-BESSEL (SFB) EXPANSION

2.1 Theory

Spherical coordinates are a natural choice for the analysis of cosmological data as they can, by an appropriate choice of basis, be used to place an observer at the origin of the analysis. Upcoming wide-field BAO surveys will provide both large and deep coverage of the sky and we therefore require a simultaneous treatment of the extended radial coverage and spherical sky geometry. For this problem, the sFB expansion is a natural basis for the analysis of random fields in such a survey.

We introduce a homogeneous 3D random field $\Psi(\hat{\Omega}, r)$ with $\hat{\Omega}$ defining a position on the surface of a sphere and r denoting the comoving radial distance. The eigenfunctions of the Laplacian operators are constructed from products of the spherical Bessel functions of the first kind $j_\ell(kr)$ and spherical harmonics $Y_{\ell m}(\hat{\Omega})$ with eigenvalues of $-k^2$ for a 2-sphere. Assuming a flat background Universe, the sFB decomposition of our random field (Binney and Quinn 1991; Fisher et al 1995; Heavens and Taylor 1995; Castro, Heavens and Kitching 2005) is given by:

$$\Psi(\hat{\Omega}, r) = \sqrt{\frac{2}{\pi}} \int dk \sum_{\{\ell m\}} \Psi_{\ell m}(k) k j_\ell(kr) Y_{\ell m}(\hat{\Omega}), \quad (1)$$

and the corresponding inverse relation given by:

$$\Psi_{\ell m}(k) = \sqrt{\frac{2}{\pi}} \int d^3 \mathbf{r} \Psi(\mathbf{r}) k j_\ell(kr) Y_{\ell m}^*(\hat{\Omega}). \quad (2)$$

In our notation, $\{\ell m\}$ are quantum numbers and \mathbf{k} represents the wavenumber.¹⁰

Note that the 3D harmonic coefficients, $\Psi_{\ell m}(k)$ are a function of the radial wavenumber k . This decomposition can be viewed as the spherical polar analogy to the conventional Cartesian Fourier decomposition defined by:

$$\Psi(\mathbf{r}) = \frac{1}{(2\pi)^{3/2}} \int d^3 k \Psi(k) e^{i\mathbf{k}\cdot\mathbf{r}}, \quad (3)$$

$$\Psi(\mathbf{k}) = \frac{1}{(2\pi)^{3/2}} \int d^3 x \Psi(\mathbf{r}) e^{-i\mathbf{k}\cdot\mathbf{r}}. \quad (4)$$

¹⁰ We follow the same conventions as Leistedt et al (2011); Rassat and Refregier (2012); Castro, Heavens and Kitching (2005) but have made the substitutions $f(\mathbf{r}) \rightarrow \Psi(\mathbf{r})$ and $W_\ell(k_1, k_2) \rightarrow I_\ell^{(0)}(k_1, k_2)$.

The Fourier power spectrum, $P_{\Psi\Psi}$, is defined as the 2-point correlation function of the Fourier coefficients $\Psi(k)$:

$$\langle \Psi(\mathbf{k}) \Psi^*(\mathbf{k}') \rangle = (2\pi)^3 P_{\Psi\Psi}(k) \delta^3(\mathbf{k} - \mathbf{k}'). \quad (5)$$

Similarly we can define a 3D sFB power spectrum, $C_\ell(k)$, of our random field by calculating the 2-point correlation function of the 3D harmonic coefficients:

$$\langle \Psi_{\ell m}(k) \Psi_{\ell' m'}^*(k') \rangle = C_\ell(k) \delta^{1D}(k - k') \delta_{\ell\ell'}^K \delta_{mm'}^K. \quad (6)$$

It is possible to relate the Fourier coefficients $\Psi(\mathbf{k})$ with their sFB analog $\Psi_{\ell m}(k)$ through the following expression

$$\Psi_{\ell m}(k) = \frac{i^\ell k}{(2\pi)^{3/2}} \int d\Omega_k \Psi(\mathbf{k}) Y_{\ell m}(\hat{\Omega}_k) \quad (7)$$

where the angular position of the wave vector \mathbf{k} in Fourier space is denoted by the unit vector $\hat{\Omega}(\theta_k, \phi_k)$. The Rayleigh-expansion of a plane wave is particularly useful in connecting the spherical harmonic description with the 3D Cartesian expression. The second expression we present here is derived by differentiating the first and will be used in the derivation of RSD:

$$e^{i\mathbf{k}\cdot\mathbf{r}} = 4\pi \sum_{\ell m} i^\ell j_\ell(kr) Y_{\ell m}(\hat{\Omega}_k) Y_{\ell m}(\hat{\Omega}); \quad (8)$$

$$i(\hat{\Omega}_k \cdot \hat{\Omega}) e^{i\mathbf{k}\cdot\mathbf{r}} = 4\pi \sum_{\ell m} i^\ell j'_\ell(kr) Y_{\ell m}(\hat{\Omega}_k) Y_{\ell m}(\hat{\Omega}). \quad (9)$$

In general the radial eigenfunctions are ultra-spherical Bessel functions but they can be approximated by spherical Bessel functions when the curvature of the Universe is small (e.g. Zaldarriaga, Seljak and Bertschinger (1998)). Throughout this paper we will use $j'_\ell(x)$ and $j''_\ell(x)$ to denote the first and second derivatives of $j_\ell(x)$ with respect to its argument x . The expressions for the first and second derivatives are given in Eq.(B2) and Eq.(B3). Imposing a finite boundary condition on the radial direction will result in a discrete sampling of the k -modes. This will be discussed in more detail later.

2.2 Finite Surveys

In order to consider realistic cosmological random fields, such as the galaxy density contrast, we need to take into account the partial observation effects arising from finite survey volumes. Concise discussions of this point are given in (Rassat and Refregier 2012; Asorey et al 2012) and as such we will not devote much time to this point referring the reader to the given references.

The selection function simply denotes the probability of including a galaxy within a given survey. An observed random field $\Psi^{\text{obs}}(\mathbf{r})$ can be related to an underlying 3D random field through a survey-dependent radial selection function $\phi(r)$ that modulates the underlying field:

$$\Psi^{\text{obs}}(\mathbf{r}) = \phi(r) \Psi(\mathbf{r}). \quad (10)$$

It is possible to introduce an analogous tangential selection function but we will, as per Rassat and Refregier (2012), neglect this possibility assuming that we have full sky coverage. The resulting sFB power spectrum is given by

$$C_\ell^{(00),\text{obs}}(k_1, k_2) = \left(\frac{2}{\pi}\right)^2 \int k'^2 dk' I_\ell^{(0)}(k_1, k') I_\ell^{(0)}(k_2, k') P_{\delta\delta}(k') \quad (11)$$

where the modified window function is given by:

$$I_\ell^{(0)}(k, k') = \int dr r^2 \phi(r) k j_\ell(kr) j_\ell(k'r). \quad (12)$$

The sFB power spectrum tends to rapidly decay as we move away from the diagonal $k = k'$ and it will often be much more useful to focus purely on the diagonal contribution $C_\ell^{(00)}(k, k)$.

3 REDSHIFT SPACE DISTORTIONS

The measured distribution of galaxies is not without limits though as various systematic and survey dependent errors become more important. In practice, the observed galaxy redshift distributions are distorted due to the peculiar velocity of each galaxy. The anisotropies generated by the peculiar velocities are known as *redshift space distortions*. Although this distortion of the measured redshifts will necessarily complicate the cosmological interpretation of the spectroscopic galaxy surveys, RSD are currently one of the most optimistic probes for the measurement of the growth rate of structure formation and, as a result, an interesting probe of models for dark energy and modified theories of gravity.

The effect of RSD on the matter power spectrum can be split into two effects, the Kaiser effect and the FoG effect. The Kaiser effect corresponds to the coherent distortion of the peculiar velocity along the line of sight with an amplitude controlled by the growth-rate parameter, leading to an enhancement of the power spectrum amplitude at small k (Kaiser 1987). The FoG effect arises due to the random distribution of peculiar velocities leading to an incoherent contribution in which dephasing occurs and the clustering amplitude is suppressed (Jackson 1972). It is thought that the suppression of the amplitude is particularly important around the size of halo forming regions, i.e. at large k (Taruya, Nishimichi and Saito 2010).

For an isotropic structure in linear theory, the Kaiser effect means that an observer will measure more power in the radial direction than in the transverse modes. The amplitude of this distortion is modulated by the distortion parameter

$$\beta = \frac{f(\Omega_0)}{b(z)} = \frac{1}{b(z)} \frac{d \ln D(a)}{d \ln a} \approx \frac{\Omega_m^\gamma(a)}{b(z)} \quad (13)$$

where:

$$\Omega_m(a) = \frac{\Omega_{m,0}}{a^3} \frac{H_0^2}{H^2(a)} \quad (14)$$

such that a is the scale factor, $H(a)$ is the Hubble parameter, H_0 is the Hubble parameter at present time and $D(z)$ the linear growth factor for which $f(z) \equiv d \ln D / d \ln a$. In this parameterisation, γ is directly related to our theory of gravitation such that General Relativity predicts $\gamma \simeq 0.55$ and Ω_m is the usual mass density parameter (Wang and Steinhardt 1998; Linder 2005). This means that RSD can

be used to probe the growth of structure, the galaxy clustering bias function $b(z)$ as well as probing dark energy and modified theories of gravity (Guzzo et al 2008). Measuring the growth rate from RSD is a non-trivial procedure and a detailed understanding of systematic errors is crucial in order to disentangle different theories of gravity or dark energy de la Torre and Guzzo (2012). Euclid aims to constrain the growth rate parameter to the percent level but incomplete modelling of RSD introduces systematics on order 10 – 15% (Taruya, Nishimichi and Saito 2010; Okumura and Jing 2011; Bianchi et al 2012; de la Torre and Guzzo 2012). This makes the study of RSD in the sFB formalism all the more timely. In this next section we will outline some of the basic ingredients that are used in modelling RSD in Fourier space before constructing the analogous results in the sFB formalism.

3.1 RSD in Fourier Space

Before presenting the RSD in the sFB formalism we briefly review some of the key results from modelling RSD in Fourier space and the appropriate limitations that are adopted in the model.

The effect of a peculiar velocity \mathbf{v} is to distort the apparent comoving position \mathbf{s} of a galaxy from its true comoving position \mathbf{r} :

$$\begin{aligned} \mathbf{s} &= \mathbf{r} + \frac{v_{\parallel}(\mathbf{r}) \hat{n}}{aH(a)} \\ &= \mathbf{r} + f\phi(\mathbf{r}) \hat{n} \end{aligned} \quad (15)$$

where f is the linear growth rate, \hat{n} is a vector lying parallel to an observer's line of sight and v_{\parallel} is the component of the velocity parallel to the line of sight. The resulting redshift space density field $\delta_s(\mathbf{s})$ is obtained by imposing mass conservation, $[1 + \delta_s(\mathbf{s})] d^3\mathbf{s} = [1 + \delta_r(\mathbf{r})] d^3\mathbf{r}$, which results in the following:

$$[1 + \delta_s(\mathbf{s})] = [1 + \delta_r(\mathbf{r})] \left| \frac{d^3\mathbf{s}}{d^3\mathbf{r}} \right|^{-1}. \quad (16)$$

To simplify the analysis we can adopt the distant observer approximation in which we neglect the curvature of the sky and the Jacobian reduces to a term relating only to the line of sight

$$\frac{\partial s}{\partial r} = 1 + f\phi' \quad (17)$$

where a prime denotes differentiation with respect to the line of sight, i.e. parallel to \hat{n} :

$$\phi'(\mathbf{r}) = \partial_{\parallel} \left[\frac{v_{\parallel}}{faH(a)} \right]. \quad (18)$$

The redshift space density contrast can be re-written as:

$$\delta_s(\mathbf{s}) = \frac{(\delta(\mathbf{r}) - f\phi'(\mathbf{r}))}{(1 + f\phi'(\mathbf{r}))}. \quad (19)$$

Assuming an irrotational velocity field with a velocity divergence field $\theta(\mathbf{r}) = \nabla \cdot \mathbf{v}(\mathbf{r})$ we obtain the following useful relationship,

$\phi(\mathbf{r}) = -(\nabla^{-1}\theta(\mathbf{r}))'$. In Fourier space these equations simplify as $\phi'(k) = -\mu^2\theta(k)$, where we have made use of the fact that $(\nabla^{-1})'' = (k_{\parallel}/k)^2 = \mu^2$. In our notation k_{\parallel} denotes the modes parallel to the line of sight and k_{\perp} denotes modes perpendicular to the line of sight where $k^2 = k_{\parallel}^2 + k_{\perp}^2$. Scoccimarro, Couchman and Frieman (1999) the redshift space density field can be written as

$$\begin{aligned}\delta_s(k, \mu) &= \int \frac{d^3\mathbf{s}}{(2\pi)^3} e^{-i\mathbf{k}\cdot\mathbf{s}} \delta_s(\mathbf{s}) \\ &= \int \frac{d^3\mathbf{r}}{(2\pi)^3} e^{-i\mathbf{k}\cdot\mathbf{r}} e^{-ikf\mu} [\delta(\mathbf{r}) + f\mu^2\theta(\mathbf{r})]\end{aligned}\quad (20)$$

and the corresponding power spectrum as:

$$\begin{aligned}P_s(k, \mu) &= \int \frac{d^3\mathbf{r}}{(2\pi)^3} e^{-\mathbf{k}\cdot\mathbf{r}} \left\langle e^{-ikf\mu(\phi(\mathbf{r})-\phi(\mathbf{r}'))} \right. \\ &\quad \left. \times [\delta(\mathbf{r}) + f\mu^2\theta(\mathbf{r})] [\delta(\mathbf{r}') + f\mu^2\theta(\mathbf{r}')] \right\rangle.\end{aligned}\quad (21)$$

This prescription for the Fourier power spectrum has been constructed in the plane-parallel or distant observer approximation. The terms in the square brackets is the conventional Kaiser effect as described earlier. The exponential prefactor corresponds to the small-scale velocity dispersion and relates to the Fingers-of-God effect described earlier. A simplified phenomenological power spectrum was derived by Scoccimarro (2004) by assuming that the exponential prefactor may be separated from the ensemble average

$$P_s(k, \mu) = e^{-(fk\mu\sigma_v)^2} [P_{\delta\delta}(k) + 2f\mu^2 P_{\delta\theta}(k) + f^2\mu^4 P_{\theta\theta}(k)],\quad (22)$$

where σ_v is a velocity dispersion defined in Scoccimarro (2004). In the linear regime we have $P_{\delta\delta} = P_{\delta\theta} = P_{\theta\theta}$ and the velocity dispersion prefactor tends towards zero. In such a limit we simply recover the linear result of Kaiser (1987):

$$P_s(k, \mu) = [1 + 2f\mu^2 + f^2\mu^4] P_{\delta\delta}(k).\quad (23)$$

Such a limit corresponds to making a number of approximations. For example, we require that the velocity gradient is sufficient small, the density and velocity perturbations must be accurately described by the linear continuity equations, the real-space density perturbations are well described by the linear results, i.e. $\delta(\mathbf{r}) \ll 1$, such that higher-order contributions are suppressed and we also require that the small-scale velocity dispersion tends towards zero and may be neglected. Such approximations appear to hold on the largest scales and a lot of distortion features are well modelled by this approximation. It is however known that this theory breaks down as we approach the quasi-linear and non-linear regimes. The result of Scoccimarro (2004) makes certain approximations about the separability of the exponential prefactor which neglects possible coupling terms between the velocity and density fields. A lot of effort has been invested in constructing non-linear models for RSD and upcoming surveys should prove to be a fruitful testing ground for many of these models Hivon, Bouchet, Colombi, Juszkiewicz (1995); Scoccimarro, Couchman and Frieman (1999); Scoccimarro (2004); Crocce and Scoccimarro (2008); Matsubara (2008a,b); Taruya, Nishimichi, Saito and

Hiramatsu (2009); Taruya, Nishimichi and Saito (2010); Matsubara (2011); Okamura, Taruya and Matsubara (2011); Sato and Matsubara (2011); de la Torre and Guzzo (2012). We construct the RSD in the sFB formalism by first working to the linear Kaiser result and exploring the phenomenology of such an extension.

3.2 RSD in sFB Space

As previously mentioned, the effect a peculiar velocity, or a departure from the Hubble flow, $v(\mathbf{r})$ at \mathbf{r} is to introduce a distortion to the galaxy positions in the redshift space \mathbf{s} :

$$\mathbf{s}(\mathbf{r}) = \mathbf{r} + \mathbf{v}(\mathbf{r}) \cdot \hat{\Omega}.\quad (24)$$

We denote the harmonics of a field $\Psi(\mathbf{r})$ when convolved with a selection function, $\phi(s)$, by $\tilde{\Psi}_{\ell m}(k)$. These harmonics take into account the RSD:

$$\tilde{\Psi}_{\ell m}(k) = \sqrt{\frac{2}{\pi}} \int s^2 ds \int d\hat{\Omega} \phi(s) \Psi(\mathbf{r}) k j_{\ell}(ks) Y_{\ell m}^*(\hat{\Omega}).\quad (25)$$

The Fourier transform of the linearised Euler equation can be used to relate the Fourier transform of the density contrast, $\delta(\mathbf{k})$, to that of the peculiar velocity field $v(\mathbf{r})$:

$$\mathbf{v}(\mathbf{k}) = -i\beta\mathbf{k} \frac{\delta(\mathbf{k})}{k^2}\quad (26)$$

where b is the linear bias parameter. Following the procedure outlined in Heavens and Taylor (1995), we can establish a series expansion in β such that the lowest order coefficients $\Psi_{\ell m}^{(0)}(k)$ are obtained by neglecting the RSD:

$$\tilde{\Psi}_{\ell m}(k) = \tilde{\Psi}_{\ell m}^{(0)}(k) + \tilde{\Psi}_{\ell m}^{(1)}(k) + \dots;\quad (27)$$

$$\tilde{\Psi}_{\ell m}^{(0)}(k) = \sqrt{\frac{2}{\pi}} \int_0^{\infty} k' dk' \Psi_{\ell m}(k') I_{\ell}^{(0)}(k', k);\quad (28)$$

$$\tilde{\Psi}_{\ell m}^{(1)}(k) = \sqrt{\frac{2}{\pi}} \int_0^{\infty} k' dk' \Psi_{\ell m}(k') I_{\ell}^{(1)}(k', k).\quad (29)$$

The kernels $I_{\ell}^{(0)}(k', k)$ and $I_{\ell}^{(1)}(k', k)$ define the convolution and are dependent on the choice of selection function. Note that $I_{\ell}^{(0)}(k', k)$ is simply the window function we encountered previously in Eq.(12). The kernels can be shown to be:

$$I_{\ell}^{(0)}(k, k') = \int dr r^2 \phi(r) k j_{\ell}(kr) j_{\ell}(k'r)\quad (30)$$

$$I_{\ell}^{(1)}(k, k') = \frac{\beta}{k'} \int dr r^2 k \frac{d}{dr} (\phi(r) j_{\ell}(kr)) j_{\ell}'(k'r).\quad (31)$$

The lowest order corrections due to RSD are therefore encapsulated in $\tilde{\Psi}_{\ell m}^{(1)}(k)$. We can define a set of power spectra by using these harmonic coefficients:

$$\langle \Psi_{\ell m}^{\alpha}(k) \tilde{\Psi}_{\ell' m'}^{\beta*}(k') \rangle = \mathcal{C}_{\ell}^{(\alpha\beta)}(k, k') \delta_{1D}(k - k') \delta_{\ell\ell'} \delta_{mm'},\quad (32)$$

$$\langle \Psi_{\ell m}^{\alpha}(k) \tilde{\Psi}_{\ell' m'}^{\beta*}(k') \rangle = \tilde{\mathcal{C}}_{\ell}^{(\alpha\beta)}(k, k') \delta_{\ell\ell'} \delta_{mm'}.\quad (33)$$

We can construct a generalised power spectrum by using the common structure between Eq.(28) and Eq.(29):

$$\tilde{\mathcal{C}}_{\ell}^{(\alpha\beta)}(k_1, k_2) = \left(\frac{2}{\pi}\right)^2 \int k'^2 dk' I_{\ell}^{(\alpha)}(k_1, k') I_{\ell}^{(\beta)}(k_2, k') P_{\delta\delta}(k').\quad (34)$$

The total redshifted power spectrum will be given by a sum of the various contributions:

$$\tilde{C}_\ell(k_1, k_2) = \tilde{C}_\ell^{(00)}(k_1, k_2) + 2\tilde{C}_\ell^{(01)}(k_1, k_2) + \tilde{C}_\ell^{(11)}(k_1, k_2). \quad (35)$$

If we ignore the effects introduced by the selection function, i.e. set $\phi(r) = 1$, then we recover the result for the unredshifted contributions Heavens and Taylor (1995); Fisher et al (1995); Castro, Heavens and Kitching (2005):

$$C_\ell^{(00)}(k, k) = P_{\delta\delta}(k). \quad (36)$$

These expressions hold for surveys with all-sky coverage. In the presence of homogeneity and isotropy the 3D power spectrum will be independent of radial wave number ℓ . The introduction of a sky mask breaks isotropy and introduces additional mode-mode couplings, the analysis will be generalised to this case in the next section. In the above equations we neglect a number of additional non-linear terms including General Relativistic corrections, velocity terms and lensing terms. It is also possible to adopt a full non-linear approach to RSD where the non-linear spectrum has significantly more complicated angular structure than in linear theory Shaw and Lewis (2008). The RSD information will be dependent on the relative clustering amplitude of the transverse modes and the radial modes, Asorey et al (2012). Our ability to recover information and the extent to which the information radialises will naturally depend on the geometry of the survey and which modes we are able to include.

3.3 BAO Wiggles Only

The BAOs can be isolated by constructing a ratio between the observed matter power spectrum $P_{\delta\delta}^B(k)$ and a theoretical matter power spectrum $P_{\delta\delta}^{nB}(k)$ constructed from a zero-baryon (or no-wiggle) transfer function in which the oscillations do not show up (Eisenstein et al 2005). Using these two power spectra, the ratio $R^P(k)$ will reduce the dynamic range and isolates the oscillatory features of the BAOs:

$$R^P(k) = \frac{P^B(k)}{P^{nB}(k)}. \quad (37)$$

This ratio is clearly defined for the Fourier space power spectrum but an appropriate generalisation to the sFB formalism may be constructed by calculating the ratio of the angular power spectra defined in Eq. (11), with the matter power spectrum $C_\ell^B(k)$ to the angular power spectrum with the zero-baryon power spectrum $C_\ell^{nB}(k)$ (Rassat and Refregier 2012):

$$R_\ell^C(k) = \frac{C_\ell^B(k)}{C_\ell^{nB}(k)}. \quad (38)$$

It is important to note that the characterisation method (i.e. how we choose to construct our ratio) can affect the characteristic scale of the BAOs when we take into account non-linear effects. This means that care has to be taken when comparing results that implement different methods (Rassat et al 2008). As an example we could construct our ratio by using the no-wiggles transfer function of Eisenstein et al (2005)

or adopt an interpolation scheme to construct a smooth parametric curve Blake et al (2006); Percival et al (2007); Seo and Eisenstein (2007). A different choice of smoothed matter power spectra, cosmological parameters, growth history or similar can impact the phenomenological behaviour of the underlying physics (e.g. location of BAO peaks). Other methods for characterising the acoustic oscillation scales can be found, for example, in (Percival et al 2007; Nishimichi et al 2007).

3.4 Results: RSD

In Figure [1] we compare $\tilde{C}_\ell(k)$ against a linear redshift space power spectrum, $P_s(k)$, spectra for $\ell = 5, 50$ at two given surveys corresponding to $r = 100, 1400h^{-1}$ Mpc. In this plot the ratios are constructed by considering the differences between the appropriate spectra. The following ratios have been used:

$$R_\ell^{C, \text{RSD}}(k) = \frac{C_\ell^{\text{RSD, Lin, B}}(k)}{C_\ell^{\text{RSD, Lin, nB}}(k)} \quad (39)$$

$$R_\ell^{C, \text{nRSD}}(k) = \frac{C_\ell^{\text{nRSD, Lin, B}}(k)}{C_\ell^{\text{nRSD, Lin, nB}}(k)} \quad (40)$$

$$R^{P, \text{RSD}}(k) = \frac{P^{\text{RSD, Lin, B}}(k)}{P^{\text{RSD, Lin, nB}}(k)} = R^{P, \text{nRSD}}(k). \quad (41)$$

In Figure [1], the blue line corresponds to Eq.(39), the purple line to Eq.(40) and the red line to Eq.(41). Figures [6, 7, 9] correspond to Eq.(39).

The redshift space Fourier power spectrum is simply the result derived in Kaiser (1987) and corresponds to:

$$P^s(k, \mu) = [1 + 2\mu^2 f + \mu^4 f^2] P(k). \quad (42)$$

In this linear limit, the redshift space ratio $R_s(k)$ tends to the real space ratio $R(k)$ as the linear prefactors corresponding to the redshift space corrections cancel. It is apparent that in Figure [1] the sFB spectra are damped relative to the power spectra. This arises due to mode-mixing contributions inherent when working with the sFB formalism. The unredshifted contributions are constructed from products of Bessel functions that form an orthogonal basis and there is no radial mode-mixing. When introducing RSD the higher-order terms are decomposed with respect to products involving derivatives of the spherical Bessel functions which does not form a perfectly orthogonal set of basis functions. As a result of RSD, off-diagonal elements will be generated and there is now coupling between modes. This radial mode-mixing is an intrinsic geometrical artifact of RSD on large scales and carries a distinctive damping signature (Heavens and Taylor 1995; Zaroubi and Hoffman 1996; Shapiro, Crittenden and Percival 2011). Such a mode-mixing term is not present in the Kaiser analysis where the basis functions are plane waves which have well behaved derivatives that maintain the orthogonality of the basis. In the deep survey limit it is seen that the redshift space sFB spectra do tend towards their Fourier spectra counterparts in terms of the shape, amplitude and phase albeit with the presence of the distinctive damp-

ing generated by mode-mixing which is predominantly seen at small scales and hence large k .

The effects of RSD can be seen in Figures [6-7] in comparison to the equivalent configurations without the presence of RSD in Figures [4-5]. A lower dynamical range comparison is presented in Figures [8-9] to enhance the impact that RSD have on the BAO. Note the enhanced power at low ℓ and k as well as some level of fuzziness introduced by the mode mixing. The peak amplitudes are damped at low ℓ and all the features can be seen in the corresponding slice plots of Figure [1]. In a future paper we will consider the hierarchy of multipole moments in Fourier space RSD and how measures constructed from the multipole moments can be related to RSD in the sFB formalism.

4 REALISTIC SURVEYS

The results that have been discussed above are somewhat idealised in the sense that we assume all-sky coverage with no noise. In realistic surveys we will often need to take into account the presence of a mask (relating to partial sky-coverage) and noise. If the noise is inhomogeneous we will be presented with a further complication. For partial sky coverage we find mode-mode couplings in the harmonic domain that result in the individual masked harmonics being described by a linear combination of our idealised all-sky harmonics. We do not discuss the role of partial sky-coverage in much detail but do present results generalising our formalism to include a survey mask.

4.1 Partial-Sky Coverage and Mode Mixing

Large scale surveys do not, generally, have full-sky coverage. Instead the information regarding sky-coverage is encapsulated in a mask $\chi(\hat{\Omega})$ which is unity for areas covered in the survey and zero for regions outside the survey. The field harmonics are therefore modulated in the presence of a mask:

$$\tilde{\Psi}_{\ell m}(k) = \sqrt{\frac{2}{\pi}} \int s^2 ds \int d\hat{\Omega} \left[\phi(s)\chi(\hat{\Omega}) \right] \Psi(\mathbf{r}) j_\ell(ks) Y_{\ell m}^*(\hat{\Omega}). \quad (43)$$

The convolved power-spectra in the presence of the mask takes the following form:

$$\begin{aligned} \tilde{\mathcal{C}}_\ell^{(\alpha\beta)}(k_1, k_2) &= \left(\frac{2}{\pi}\right)^2 \sum_{\ell_a} \sum_{\ell_b} \int k' dk' \int k'' dk'' \\ &\times W_{\ell\ell_a}^{(\alpha)}(k_1, k') W_{\ell\ell_b}^{(\beta)}(k_2, k'') \frac{I_{\ell\ell_a\ell_b}}{(2\ell+1)} \mathcal{C}_{\ell_a}^X \mathcal{C}_{\ell_b}^X(k', k''); \quad (44) \\ \mathcal{C}_\ell^X &= \langle \chi_{\ell m} \chi_{\ell m}^* \rangle \quad (45) \end{aligned}$$

where $I_{\ell_1\ell_2\ell_3}$ is the Gaunt integral (see Eq.(B4) of Appendix-B). The convolved power spectrum is a linear combination of all-sky spectra and depends on the power spectrum of the adopted mask (see Appendix-D for detailed derivations.).

4.2 Photometric Error Estimates

The radial coordinates from a survey are typically provided as a photometric redshift with some given error, we denote this estimated radial coordinate by \tilde{r} and let r represent the true coordinate. Following Heavens (2003), we relate the two coordinates by a conditional probability that we model as a Gaussian:

$$p(\tilde{r}|r) d\tilde{r} = \frac{1}{\sqrt{2\pi}\sigma_z} \exp\left[-\frac{(z_{\tilde{r}} - z_r)^2}{2\sigma_z^2}\right] dz_{\tilde{r}} \quad (46)$$

where $z_{\tilde{r},r}$ are the redshifts associated with the given coordinate and σ_z is the error. We assume that the error has values, $\sigma_z \sim 0.02 - 0.1$ or more and it is important to note that σ_z may vary with redshift. We can now construct harmonics that represent the average value of the expansion coefficients by using the relation between the estimated distance from photometric redshifts, \tilde{r} , and the true distance r in terms of the conditional probability:

$$\Psi_{\ell m}(k) = \sqrt{\frac{2}{\pi}} \int d^3\tilde{\mathbf{r}} \int \mathbf{r} p(\tilde{r}|r) \Psi(\mathbf{r}) k j_\ell(k\tilde{r}) Y_{\ell m}^*(\hat{\Omega}). \quad (47)$$

Such a Gaussian error leads to photometric redshift smoothing.

4.3 Error Estimate

The signal to noise for individual modes for a given power-spectrum can be expressed as:

$$\frac{\delta\mathcal{C}_\ell(k, k)}{\mathcal{C}_\ell(k, k)} = \sqrt{\frac{2}{2\ell+1}} \left(1 + \frac{1}{\bar{n}\mathcal{C}_\ell(k, k)}\right) \quad (48)$$

Where \bar{n} is the average number density of galaxies and the second term represents the leading order shot-noise contribution. For our results we take $\bar{n} = 10^{-3} h^3 \text{Mpc}^{-3}$.

5 NON-LINEAR CORRECTIONS

The role of nonlinear gravitational clustering can be investigated in the sFB formalism by incorporating higher-order corrections to the power spectrum as described in perturbation theory. The approach we adopt here is standard perturbation theory (SPT), also known as Eulerian perturbation theory, which provides a rigorous framework from which we can investigate the structure of the sFB spectra in a fully analytic manner (Vishniac 1983; Fry 1984; Goroff, Grinstein, Rey and Wise 1986; Suto and Sasaki 1991; Makino, Sasaki and Suto 1992; Jain and Bertschinger 1994; Scoccimarro and Frieman 1996). Standard perturbation theory is one of the most straightforward approaches to studies beyond linear theory and is based on a series solution to the hydrodynamical fluid equations in powers of an initial density or velocity field. The nonlinear clustering of matter arises from mode-mode couplings of density fluctuations and velocity divergence as seen from the Fourier space equations. The role of perturbation theory in the nonlinear evolution of the BAO in the power spectrum has been previously investigated (for an incomplete selection of references please see: Jeong and Komatsu (2006); Nishimichi

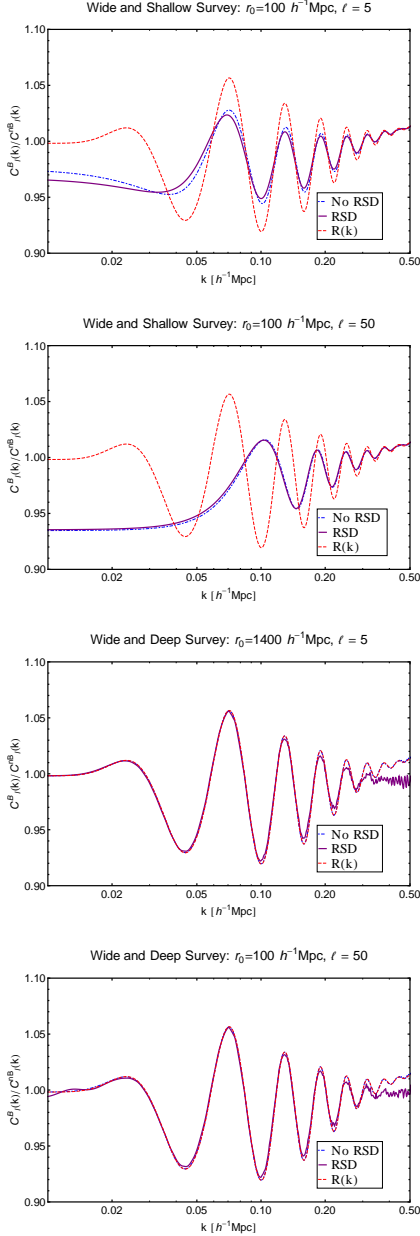


Figure 1. Slice in l -space showing $R_l^C(k)$ for a wide and shallow survey of $r_0 = 100h^{-1}Mpc$ at $\ell = 5$ (1st panel) and $\ell = 50$ (2nd panel) and for a wide and deep survey of $r_0 = 1400h^{-1}Mpc$ at $\ell = 5$ (3rd panel) and $\ell = 50$ (4th panel). The blue line denotes the $C^{(00)}$ term, the purple line the sFB spectra incorporating RSD and the red line shows the Fourier space power spectra. In the linear regime the linear prefactors for RSD in the Fourier power spectra cancel and the results correspond to the unredshifted Fourier space power spectra.

et al (2007); Nomura, Yamamoto and Nishimichi (2008); Nomura, Yamamoto, Huetsi and Nishimichi (2009); Taruya, Nishimichi, Saito and Hiramatsu (2009); Taruya, Nishimichi and Saito (2010)). In this paper we generalise these investigations to the sFB approach. The redshift of the Fourier space power spectra was taken to be $z \sim 0.2$ and the effects of growth have not been analysed in detail. For small surveys the growth does not seem to have significant effects.

5.1 Standard Perturbation Theory

Consider the hydrodynamic equations of motion for density perturbations δ such that our comoving coordinates are denoted by \mathbf{x} and the conformal time by η :

$$\delta'(\mathbf{x}, \eta) + \nabla \cdot [(1 + \delta(\mathbf{x}, \eta))\mathbf{v}(\mathbf{x}, \eta)] = 0, \quad (49)$$

$$\mathbf{v}'(\mathbf{x}, \eta) + [\mathbf{v}(\mathbf{x}, \eta) \cdot \nabla] \mathbf{v}(\mathbf{x}, \eta) + \mathcal{H}(\eta)\mathbf{v}(\mathbf{x}, \eta) = -\nabla\phi(\mathbf{x}, \eta), \quad (50)$$

$$\nabla^2\phi(\mathbf{x}, \eta) = \frac{3}{2}\mathcal{H}^2(\eta)\delta(\mathbf{x}, \eta), \quad (51)$$

where a prime denotes the derivative with respect to the conformal time and $\mathcal{H} = a'/a$. The rotational mode of the peculiar velocity \mathbf{v} is a decaying solution in an expanding universe and can be neglected in this approach. We introduce a scalar field describing the velocity divergence:

$$\Theta(\mathbf{x}, \eta) = \nabla \cdot \mathbf{v}(\mathbf{x}, \eta). \quad (52)$$

In our discussion we will focus on a description of the density perturbations and Fourier decompose the above equations to set up and solve a system of integro-differential equations. The Fourier decomposition of the perturbations are defined by:

$$\delta(\mathbf{x}, \eta) = \int \frac{d^3k}{(2\pi)^3} \delta(\mathbf{k}, \eta) e^{-i\mathbf{k}\cdot\mathbf{x}}, \quad (53)$$

$$\Theta(\mathbf{x}, \eta) = \int \frac{d^3k}{(2\pi)^3} \Theta(\mathbf{k}, \eta) e^{-i\mathbf{k}\cdot\mathbf{x}} \quad (54)$$

The equations of motion can be decomposed as follows:

$$\delta'(\mathbf{x}, \eta) + \Theta(\mathbf{k}, \eta) = - \int d^3k_1 \int d^3k_2 \delta^{(3)}(\mathbf{k}_1 + \mathbf{k}_2 - \mathbf{k}) \frac{\mathbf{k} \cdot \mathbf{k}_1}{k_1^2} \Theta(\mathbf{k}_1, \eta) \delta(\mathbf{k}_2, \eta), \quad (55)$$

$$\Theta'(\mathbf{k}, \eta) + \mathcal{H}(\eta)\Theta(\mathbf{k}, \eta) + \frac{3}{2}\mathcal{H}^2(\eta)\delta(\mathbf{k}, \eta) = - \int d^3k_1 \int d^3k_2 \delta^{(3)}(\mathbf{k}_1 + \mathbf{k}_2 - \mathbf{k}) \frac{k^2(\mathbf{k}_1 \cdot \mathbf{k}_2)}{2k_1^2k_2^2} \Theta(\mathbf{k}_1, \eta)\Theta(\mathbf{k}_2, \eta). \quad (56)$$

In order to solve these coupled integro-differential equations we introduce a perturbative expansion of our variables:

$$\delta(\mathbf{k}, \eta) = \sum_{n=1}^{\infty} a^n(\eta) \delta_n(\mathbf{k}), \quad (57)$$

$$\Theta(\mathbf{k}, \eta) = \mathcal{H}(\eta) \sum_{n=1}^{\infty} a^n(\eta) \Theta_n(\mathbf{k}). \quad (58)$$

The general n-th order solutions are given by:

$$\delta_n(\mathbf{k}) = \int d^3q_1 \dots \int d^3q_n \delta^{(3)}\left(\sum_{i=1}^n \mathbf{q}_i - \mathbf{k}\right) \times F_n(\mathbf{q}_1, \dots, \mathbf{q}_n) \Pi_{i=1}^n \delta_1(\mathbf{q}_i), \quad (59)$$

$$\Theta_n(\mathbf{k}) = - \int d^3q_1 \dots \int d^3q_n \delta^{(3)}\left(\sum_{i=1}^n \mathbf{q}_i - \mathbf{k}\right) \times G_n(\mathbf{q}_1, \dots, \mathbf{q}_n) \Pi_{i=1}^n \delta_1(\mathbf{q}_i), \quad (60)$$

where the kernels $F_n(\mathbf{q}_1, \dots, \mathbf{q}_n)$ and $G_n(\mathbf{q}_1, \dots, \mathbf{q}_n)$ are given by Jain and Bertschinger (1994):

$$F_n(\mathbf{q}_1, \dots, \mathbf{q}_n) = \sum_{m=1}^{n-1} \frac{G_m(\mathbf{q}_1, \dots, \mathbf{q}_m)}{(2n+3)(n-1)} \times \left[(1+2n) \frac{\mathbf{k} \cdot \mathbf{k}_1}{k_1^2} F_{n-m}(\mathbf{q}_{m+1}, \dots, \mathbf{q}_n) + \frac{k^2(\mathbf{k}_1 \cdot \mathbf{k}_2)}{k_1^2 k_2^2} G_{n-m}(\mathbf{q}_{m+1}, \dots, \mathbf{q}_n) \right], \quad (61)$$

$$G_n(\mathbf{q}_1, \dots, \mathbf{q}_n) = \sum_{m=1}^{n-1} \frac{G_m(\mathbf{q}_1, \dots, \mathbf{q}_m)}{(2n+3)(n-1)} \times \left[3 \frac{\mathbf{k} \cdot \mathbf{k}_1}{k_1^2} F_{n-m}(\mathbf{q}_{m+1}, \dots, \mathbf{q}_n) + n \frac{k^2(\mathbf{k}_1 \cdot \mathbf{k}_2)}{k_1^2 k_2^2} G_{n-m}(\mathbf{q}_{m+1}, \dots, \mathbf{q}_n) \right], \quad (62)$$

The kernel $F_n(\mathbf{q}_1, \dots, \mathbf{q}_n)$ is not symmetric under permutations of the argument $\mathbf{q}_1 \dots \mathbf{q}_n$ and must be symmetrised:

$$F_n^{(s)} = \frac{1}{n!} \sum_{\text{Permutations}} F_n(\mathbf{q}_1, \dots, \mathbf{q}_n). \quad (63)$$

As an example, the second order symmetrised solution is given by:

$$F_2^{(s)}(k_1, k_2) = \frac{5}{7} + \frac{2}{7} \frac{(\mathbf{k}_1 \cdot \mathbf{k}_2)^2}{k_1^2 k_2^2} + \frac{(\mathbf{k}_1 \cdot \mathbf{k}_2)}{2} \left(\frac{1}{k_1^2} + \frac{1}{k_2^2} \right). \quad (64)$$

The corresponding second order matter power spectrum represents the linear matter power spectrum plus the additional higher-order corrections. This calculation is made under the assumption that the first order density perturbations $\delta_1(\mathbf{k})$ constitute a Gaussian random field. The power spectrum up to second order is given by:

$$P_{\text{SPT}}(k, z) = D^2(z) P_{\text{lin}}(k) + D^4(z) P_2(k), \quad (65)$$

where P_{lin} is the conventional linear matter power spectrum and the second order correction are given by:

$$P_2(k) = P_{22}(k) + 2P_{13}(k). \quad (66)$$

These terms correspond to the contributions to the 4-point correlation function from the (2,2)-order and the (1,3)-order cross-correlations.

The explicit form of these terms are given by:

$$P_{22}(k) = 2 \int d^3q P_{\text{lin}}(|\mathbf{k} - \mathbf{q}|) [F_2^s(\mathbf{q}, \mathbf{k} - \mathbf{q})]^2, \quad (67)$$

$$P_{13}(k) = 3P_{\text{lin}}(q) \int d^3q P_{\text{lin}}(q) F_3^s(\mathbf{q}, -\mathbf{q}, \mathbf{k}) \quad (68)$$

and the full equations are presented in Appendix C.

It should be noted that the analytical predictions arising from standard perturbation theory will eventually break down as the non-linear terms become dominant over the linear theory predictions. Jeong and Komatsu (2006) demonstrated that one-loop standard perturbation theory was able to fit N-body simulations to greater than 1% accuracy when the maximum wave number $k_{1\%}$ satisfies (Taruya, Nishimichi, Saito and Hiramatsu 2009):

$$\frac{k_{1\%}^2}{6\pi^2} \int_0^{k_{1\%}} dq P_{\text{lin}}(q; z) = C \quad (69)$$

where $C = 0.18$ in standard perturbation theory. SPT theory relies on a straightforward expansion of the set of cosmological hydrodynamical equations and the approach has been repeatedly noted as being insufficiently accurate to model and describe the BAOs (Jeong and Komatsu 2006; Taruya, Nishimichi, Saito and Hiramatsu 2009; Nishimichi et al 2009; Carlson, White and Padmanabhan 2009; Taruya, Nishimichi and Saito 2010). In particular the amplitude of SPT predicts a monotonical increase with wavenumber that overestimates the amplitude (Figure [2]) with respect to N-body simulations Taruya, Nishimichi, Saito and Hiramatsu (2009). This is also seen in the full (k, ℓ) space spectra in Figures [10-11].

5.2 Results: SPT

In Figures [10-11] we have divided the nonlinear power spectrum by a linear no-baryon power spectrum when constructing the ratio $R_\ell^C(k)$ highlighting the scale dependence introduced by mode coupling. An alternative possibility would be to divide the nonlinear power spectrum P^{NL} by a power spectrum constructed from smoothing the nonlinear spectrum $P_{\text{smooth}}^{\text{NL}}$ that removes the scale dependence and allows for a more detailed comparison of PT predictions against numerical simulations. We construct the ratios as follows:

$$R_\ell^{C, \text{NL/SPT}}(k) = \frac{C_\ell^{\text{NL/SPT,B}}(k)}{C_\ell^{\text{Lin,nB}}(k)} \quad (70)$$

$$R_\ell^{C, \text{Lin}}(k) = \frac{C_\ell^{\text{Lin,B}}(k)}{C_\ell^{\text{Lin,nB}}(k)} \quad (71)$$

$$R^{P, \text{NL/SPT}}(k) = \frac{P^{\text{NL/SPT,B}}(k)}{P^{\text{Lin,nB}}(k)} \quad (72)$$

In Figure [2] the blue spectra corresponds to Eq.(70), the purple spectra to Eq.(71) and the red spectra to Eq.(72). These spectra do not incorporate RSD. In Figures[10-11] the ratio Eq.(70) is used.

5.3 Lagrangian Perturbation Theory

LPT (Matsubara 2008a) provides a description of the formation of structure by relating the Eulerian coordinates, \mathbf{x} , to comoving coordinates, \mathbf{q} , through the displacement field $\Psi(\mathbf{q}, t)$:

$$\mathbf{x}(\mathbf{q}, t) = \mathbf{q} + \Psi(\mathbf{q}, t). \quad (73)$$

With the assumption that the initial density field is sufficiently uniform, the Eulerian density field $\rho(\mathbf{x})$ will satisfy the continuity relation $\rho(\mathbf{x}) d^3x = \bar{\rho} d^3q$ where we have denoted the mean density in comoving coordinates by $\bar{\rho}$. The fraction densities will then be given by:

$$\delta(\mathbf{x}) = \int d^3q \delta^3[\mathbf{x} - \mathbf{q} - \Psi(\mathbf{q})] - 1, \quad (74)$$

$$\delta(\mathbf{k}) = \int d^3q e^{-i\mathbf{k}\cdot\mathbf{q}} \left[e^{-i\mathbf{k}\cdot\Psi(\mathbf{q})} - 1 \right]. \quad (75)$$

Assuming a pressureless self-gravitating Newtonian fluid in an expanding FLRW universe, the equations of motion for the displacement field are given by Matsubara (2008a):

$$\frac{d^2}{dt^2} \Psi + 2H \frac{d}{dt} \Psi = -\nabla_{\mathbf{x}} \phi[\mathbf{q} + \Psi(\mathbf{q})], \quad (76)$$

where ϕ is the gravitation potential as determined by Poisson's equation: $\nabla_{\mathbf{x}}^2 \phi(\mathbf{x}) = 4\pi G \bar{\rho} a^2 \delta(\mathbf{x})$. LPT proceeds by performing a perturbative series expansion of the displacement field:

$$\Psi = \Psi^{(1)} + \Psi^{(2)} + \dots \quad (77)$$

$$\Psi^{(N)} = \mathcal{O}\left([\Psi^{(1)}]^N\right) \quad (78)$$

The perturbative terms in the series expansion can be written schematically as:

$$\begin{aligned} \tilde{\Psi}^{(n)}(p) &= \frac{i}{n!} D^n(t) \int \frac{d^3p_1}{(2\pi)^3} \cdot \frac{d^3p_n}{(2\pi)^3} \delta^3\left(\sum_{j=1}^n p_j - p\right) \\ &\times L^{(n)}(p_1, \dots, p_n) \delta_0(p_1) \cdots \delta_0(p_n). \end{aligned} \quad (79)$$

We can perform a similar expansion for both the fractional density and the power spectrum, further details can be found in Matsubara (2008a) and we will just introduce the results for the power spectrum and how it relates to the predictions of SPT. The power spectrum can be written as:

$$P(k) = \int d^3q e^{-i\mathbf{k}\cdot\mathbf{q}} \left(\left\langle e^{-i\mathbf{k}\cdot[\Psi(\mathbf{q}_1) - \Psi(\mathbf{q}_2)]} \right\rangle - 1 \right). \quad (80)$$

The two main types of terms that we find in these equations are those terms that depend only on a single position, which are factored out into the first exponential term, and those terms that depend on some separation between positions, as seen in the second exponential term. Using the cumulant expansion theorem the power spectrum can be written as:

$$\begin{aligned} P(k) &= \exp \left[-2 \sum_{n=1}^{\infty} \frac{k_{i_1} \cdot k_{i_{2n}}}{(2n)!} A_{i_1 \cdot i_{2n}}^{(2n)} \right] \\ &\times \int d^3q e^{-i\mathbf{k}\cdot\mathbf{q}} \left\{ \exp \left[\sum_{N=2}^{\infty} \frac{k_{i_1} \cdot k_{i_N}}{(N!)} B_{i_1 \cdot i_N}^{(N)}(q) \right] - 1 \right\} \end{aligned} \quad (81)$$

where $A_{i_1 \cdot i_{2n}}^{(2n)}$ and $B_{i_1 \cdot i_N}^{(N)}$ are given in Matsubara (2008a). $A^{(N)}$ relates to the cumulant of a displacement vector at a single position and $B^{(N)}$ relates to the cumulant of two displacement vectors separated by $|\mathbf{q}|$. Expanding both the $A^{(N)}$ and the $B^{(N)}$ terms yields SPT. Matsubara (2008a), however, proposes expanding only the $B^{(N)}$ terms and leaving the $A^{(N)}$ terms as an exponential prefactor. The justification for this is that this exponential prefactor will contain infinitely higher-order perturbations in terms of SPT and has effectively given a way to resum the infinite series of perturbations found in SPT. Expanding and solving for the $B^{(N)}$ terms yields the standard LPT results Matsubara (2008a):

$$P(k) = e^{-(k\Sigma)^2/2} \left[P_{\text{lin}}(k) + P_{22}(k) + P_{13}^{\text{LPT}}(k) \right]. \quad (82)$$

The term P_{22} is identical to its SPT counterpart but the term P_{13}^{LPT} is now slightly modified but retains much of the structure found in SPT.

5.4 Results: LPT

In Figures [12-13] we again divide the nonlinear power spectrum by a linear no-baryon power spectrum when constructing the ratio $R_{\ell}^C(k)$. The explicit ratios used are:

$$R_{\ell}^{C, \text{NL/LPT}}(k) = \frac{C_{\ell}^{\text{NL/LPT,B}}(k)}{C_{\ell}^{\text{Lin,nB}}(k)} \quad (83)$$

$$R_{\ell}^{C, \text{Lin}}(k) = \frac{C_{\ell}^{\text{Lin,B}}(k)}{C_{\ell}^{\text{Lin,nB}}(k)} \quad (84)$$

$$R^{P, \text{NL/LPT}}(k) = \frac{P^{\text{NL/LPT,B}}(k)}{P^{\text{Lin,nB}}(k)} \quad (85)$$

In Figure [3] the blue spectra corresponds to Eq.(83), the purple spectra to Eq.(84) and the red spectra to Eq.(85). These spectra do not incorporate RSD. In Figures[12-13] the ratio Eq.(83) is used.

The sFB can be seen to mimic the predictions of LPT in consistently underestimating the power at large k but we also see that the sFB power spectra radialise towards the non-linear LPT spectra in the limit $r \rightarrow \infty$. This can be seen in Figure [3] where the non-linear sFB tends towards the Fourier space power spectrum in amplitude and phase. We have included a comparison to the linear sFB spectra, which we know to radialise to the linear Fourier space spectra. This behaviour is completely expected due to the nature of the sFB formalism and the fact that the resulting angular spectra are still constructed via products of Bessel functions which form an orthogonal set of basis functions. As such we do not observe the types of mode-mixing that are inherent when considering RSD in the sFB formalism. The damping and smearing of the BAOs in this instance is purely from

gravitational instability and is encapsulated in the power spectrum. We also note that the full (ℓ, k) plane is an interesting arena for visualising some of the differences in behaviour between various models for structure formation. This can be seen in the changes to the widths and amplitudes of the BAO wiggles as seen in the plane in Figures [10-13].

As future wide field surveys will cover both wide and deep regions of the sky we can use the sFB formalism as a tool to distinguish between different models for non-linear evolution of the matter density field. Interesting questions include, how do different theories affect the distribution of power in the radial and tangential modes? How can the sFB formalism be expanded to compare the RSD results to those as derived from higher-order perturbation theory? How can we best characterise the sFB spectra and how can we characterise the radialisation of information in these higher-order models? The analysis and results to these questions will be presented in a forthcoming paper.

6 RESULTS

Following Rassat and Refregier (2012) we construct the quantity $R_\ell^C(k)$ to isolate the BAOs in the sFB formalism. The matter power spectrum includes the physical effects of baryons leading to the characteristic oscillations as seen in Fourier space (Sunyaev and Zel'dovich 1970; Peebles and Yu 1970; Seo and Eisenstein 2003, 2007). In our analysis, we have adopted the zero-Baryon transfer function of Eisenstein et al (2005) to model the power spectra excluding the physical effects of baryons.

In Figure [1] we construct slices of constant ℓ through $R_\ell^C(k)$ to investigate how RSD manifest themselves in the oscillations. Rassat and Refregier (2012) used such slice plots to investigate the radialisation of information when varying levels of tangential and radial information is included in a survey. The radialisation of information can be investigated by notion that in the limit $r_0 \rightarrow \infty$ we find:

$$\lim_{r_0 \rightarrow \infty} R_\ell^C(k) = R^P(k) = \frac{P^B(k)}{P^{nB}(k)}. \quad (86)$$

Using this definition, radialisation means that $R_\ell^C(k)$ tends towards $R^P(k)$ in both phase and amplitude. This occurs as the tangential modes are attenuated due to mode-canceling along the line of sight (Rassat and Refregier 2012). The radialisation can be seen in Figures [1-3] as the amplitude and phase of the sFB spectra tends towards those of the Fourier space spectra. Additionally the BAOs appear to only have a radial (k) dependence in surveys with a large radial parameter r_0 , as can be seen by the invariance the BAOs under a varying multipole ℓ . The addition of RSD does not change this trend drastically though we do see more prominent radial and tangential dependence in Figure [1] with the rate at which the BAOs radialise being affected due to mode-mixing that leads to attenuation and peak shifts. The results appear to be in agreement with previous studies with percent level shifts in the peaks to smaller k and damping of the amplitude (Nishimichi et al 2007; Nomura, Yamamoto and Nishimichi 2008; Smith, Scoccimarro and Sheth 2008; Nomura, Yamamoto, Huetsi and Nishimichi 2009; Taruya, Nishimichi and Saito

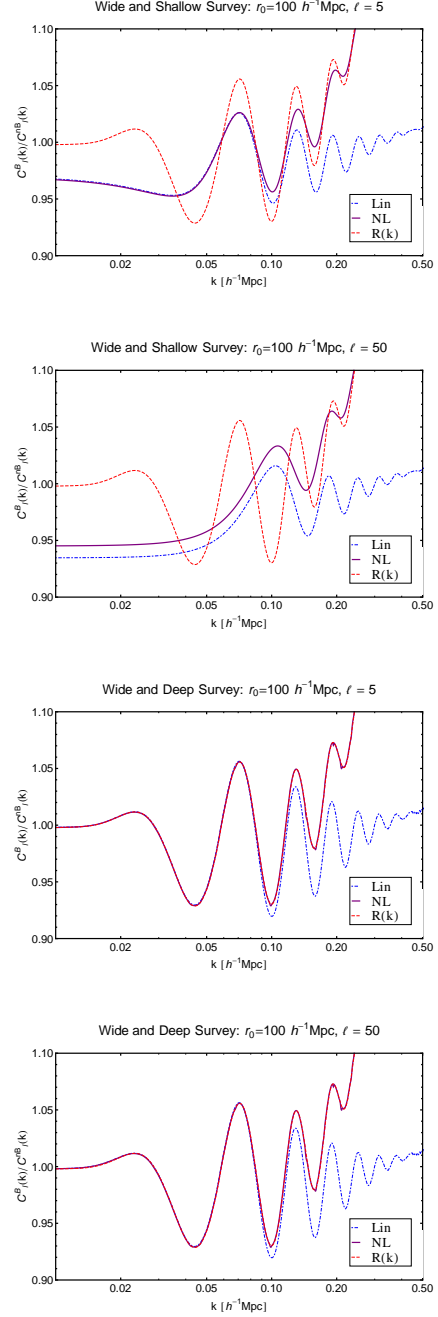


Figure 2. Slice in l -space showing $R_\ell^C(k)$ for $\ell = 5$ (top-panels) and $\ell = 50$ (bottom-panels) in a wide and shallow survey of $r_0 = 100h^{-1}\text{Mpc}$ (left-panels) as well as for a deep survey of $r_0 = 1400h^{-1}\text{Mpc}$ (right-panels). The solid blue line represents the linear angular spectra, the solid purple line the non-linear 1-loop SPT angular spectra and the dashed line the non-linear 1-loop SPT power spectrum. SPT consistently overestimates the linear power spectrum in the large- k limit and it is well known that SPT works well at high- z and large scales.

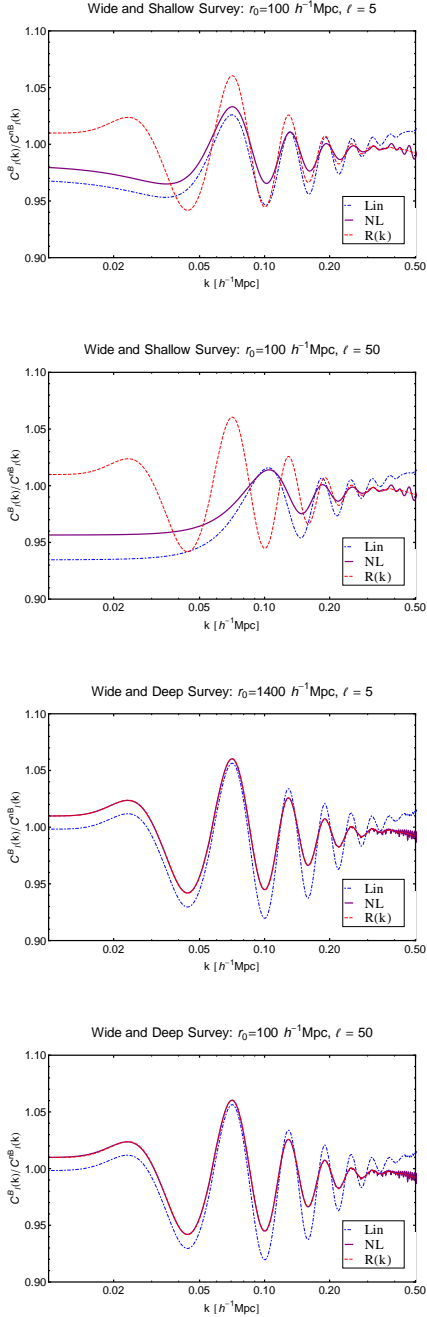


Figure 3. Slice in l -space showing $R_\ell^C(k)$ for $\ell = 5$ (top-panels) and $\ell = 50$ (bottom-panels) in a wide and shallow survey of $r_0 = 100h^{-1}\text{Mpc}$ (left-panels) and a wide and deep survey of $r_0 = 1400h^{-1}\text{Mpc}$ (right-panels). The solid blue line denotes the linear results, the solid purple line the non-linear 1-loop LPT spectra and the dashed line the non-linear 1-loop LPT spectra. LPT consistently underestimates the power spectrum in the large- k limit contrasting to the divergence at large- k in 1-loop SPT results. This difference occurs due to the effective resummation of an infinite series of perturbations from SPT that occurs in LPT.

2010). As can be seen in Figure [1] the BAOs seem to effectively radialise, even in the presence of RSD, at large values of the radius parameter r_0 and for higher multipoles ℓ . Effective radialisation simply means that the behaviour (i.e. amplitude and phase of the peaks and troughs) of the sFB spectra with RSD asymptotes towards the Fourier space spectra with RSD under the caveat that the intrinsic mode-mixing causes some smearing of radial information and leads to the distinctive damping features seen at high- k . The radialisation of information can be linked with the preservation of the orthogonality of the basis functions. In the case of RSD, the appearance of derivatives of spherical Bessel functions guarantees that the basis will not be perfectly orthogonal and we observe mode-mode coupling and the generation of off-diagonal contributions. In higher-order PT, the basis functions are still spherical Bessel functions and we observe the radialisation as per linear theory. The behaviour of the non-linear sFB spectra in the full (ℓ, k) space is naturally different for various descriptions of non-linearity in gravitational collapse.

The BAOs in the sFB formalism will radialise as the survey size, r_0 , is allowed to increase. This corresponds to the amplitude and the phase of the BAOs tending towards the values as measured in the Fourier space ratio $R^P(k)$. As noted in Rassat and Refregier (2012), for a wide-field shallow survey the BAO will have smaller amplitudes and are spread across the (ℓ, k) space. It was also shown in Rassat and Refregier (2012) that the BAOs appear to radialise before the full sFB spectrum is able to and notably so at large ℓ (Figures [4-5]) and this is one of the key motivations for implementing the sFB formalism. With the addition of RSD, the radialisation of information is intrinsically limited due to mode-mixing but a lot of the same phenomenological behaviour can be seen: dependence on radial modes and not on tangential modes at large r and the asymptotic behaviour toward the Fourier space spectra at large r .

7 CONCLUSION

The baryon acoustic oscillations give rise to a characteristic signature in the observed matter power spectrum that acts as a standard ruler. Unfortunately, the observed matter power spectrum is contaminated and complicated by the non-linear evolution of density perturbations, galaxy clustering bias, RSD and survey specific systematic errors. Additionally, upcoming future surveys will cover both large and deep areas of the sky demanding a formalism that simultaneously treats the both the spherical sky geometry and the extended radial coverage. The sFB basis was proposed as a natural basis for random fields in this geometry. The recent study by Rassat and Refregier (2012) was an initial step into investigating the role of the sFB formalism in the study and analysis of the BAO. This study, however, did not go as far as including higher-order contributions to the power spectrum that may impact the radialisation of information by introducing, for example, mode-mode couplings. The stability of this radialisation of information and the information content of tangential (ℓ) and radial (k) modes for higher-order physics is the key topic of interest.

In this paper we have presented a short treatment of the effects of **linear** RSD and non-linear corrections to measurements of baryon

acoustic oscillations in the sFB expansion. In order to guide this investigation we have extended the formalism and techniques outlined in Rassat and Refregier (2012) and the appropriate machinery for partial-sky coverage was introduced. In particular we have been able to use the procedure outlined in Heavens and Taylor (1995) to construct a series expansion solution to model RSD. This solution was used to numerically and analytically investigate the modulation to the angular sFB power spectrum. The qualitative behaviour of these corrections was outlined for surveys with varying levels of radial (k -modes) and tangential (l -modes) information. It was seen that the RSD impact the radialisation of information through mode-mixing that generates a distinct signature in the spectra. These RSD were investigated over a range of survey configurations. The mode-mode coupling was related to the presence of derivatives of spherical Bessel functions and was contrasted to the linear Kaiser result in which the basis functions are constructed from plane waves or derivatives of plane waves which simply return a plane wave of the same frequency and preserve orthogonality. This mode-mode coupling can therefore be thought of as a geometrical artifact in the sFB formalism arising from RSD on large scales Heavens and Taylor (1995); Zaroubi and Hoffman (1996); Shapiro, Crittenden and Percival (2011).

Additionally we considered the structure and form of the sFB spectra when non-linearity arising from gravitational clustering was considered. We primarily investigated one-loop corrections to the matter power spectrum arising from two mainstream models for leading order corrections as given by SPT and LPT. A brief outline of perturbation theory methods was given and the basic equations for SPT and LPT introduced. The non-linear corrections, and how we expect them to be independent of the notion of radialisation of information in the BAOs, was numerically investigated. The redshift of the Fourier space power spectrum was taken to be $z \sim 0.2$ and the detailed study of the non-linear corrections with redshift will be presented elsewhere. These are not thought to be important at low redshifts or shallow surveys where the impact of growth seems negligible.

In this paper we have neglected other contributions to the power spectrum such as General Relativistic corrections, lensing terms, the role of non-linearities through more detailed studies, more complex treatments of galaxy biasing and more detailed modelling of the hydrodynamical and radiative processes involved in these processes (Guillet et al 2010; Juszkiewicz, Hellwing and van de Weygaert 2012). In addition we have not considered the role of systematic errors associated with a given survey. It would be interesting to compare the results from SKA-like configurations and N-body simulations but we leave this to a future paper.

8 ACKNOWLEDGEMENTS

DM acknowledges support from STFC standard grant ST/G002231/1 at the School of Physics and Astronomy at Cardiff University where this work was completed. Its a pleasure to thanks Peter Coles and Alan Heavens, for many useful discussions. We note that a paper by Yoo and Desjacques (2013) appeared on the arXiv shortly after submission of this paper.

REFERENCES

- Abramo L. R., Reimberg P. H., Xavier H. S., 2010, PRD, 82, 043510, arXiv:1105.0563
- Adelman-McCarthy J. K., Agüeros M. A., Allam S. S., et al., 2008, ApJS, 175, 297
- Alam U., Sahni V., 2006, PRD, 73, 084024, arXiv:astro-ph/0511473
- Alcock C., Paczynski B., 1979, Nat., 281, 358
- Amendola L., Quercellini C., Giallongo E., 2005, MNRAS, 357, 429, arXiv:astro-ph/0404599
- Annis J., et al., The Dark Energy Task Force, 2005, arXiv:astro-ph/0510195
- Asorey J., Crocce M., Gaztanaga E., Lewis A., 2012, arXiv:1207.6487
- Banerji M., Abdalla F. B., Lahav O., Lin H., 2008, MNRAS, 386, 1219, arXiv:0711.1059v2
- Benítez N., et al., 2009, APJ, 691, 241, arXiv:0807.0535v4
- Bianchi D., Guzzo L., Branchini E., Majerotto E., de la Torre S., Marulli F., Moscardini L., Angulo R. E., 2012, MNRAS, 427, 2420-2436
- Binney J., Quinn T., 1991, MNRAS, 241, 678
- Blake C., Parkinson D., Bassett B., Glazebrook K., Kunz M., Nichol R. C., 2006, MNRAS, 365, 255, arXiv:astro-ph/0510239
- Carlson J., White M., Padmanabhan N., 2009, PRD, 80, 043531, arXiv:0905.0479
- Castro P. G., Heavens A. F., Kitching T. D., 2005, PRD, 72, 023516, arXiv:astro-ph/0503479
- Challinor A., Lewis A., 2011, PRD, 84, 043516, arXiv:1105.5292
- Coles P., Erdogdu P., 2007, JCAP, 0710, 007, arXiv:0706.0412
- Colless M., et al., 2003, arXiv:astro-ph/0306581, "The 2dF Galaxy Redshift Survey: Final Data Release"
- Crocce M., Scoccimarro R., 2008, PRD, 77, 023533
- Crocce M., Fosalba P., Castander F. J., Gaztanaga E., 2010, MNRAS, 403, 1353, arXiv:0907.0019
- Dolney D., Jain B., Takada M., 2006, MNRAS, 366, 884-898, arXiv:astro-ph/0409445
- Eisenstein D. J., Zehavi I., Hogg D. W., Scoccimarro R., et al., 2005, APJ, 633, 560, arXiv:astro-ph/0501171
- Erdogdu P., et al., 2006, MNRAS, 373, 45-64, arXiv:astro-ph/0610005
- February S., Clarkson C., Maartens R., 2012, arXiv:1206.1602
- Fisher K. B., Scharf C. A., Lahav O., 1994, MNRAS, 266, 219-226
- Fisher K. B., Lahav O., Hoffman Y., Lynden-Bell D., Zaroubi S., 1995, MNRAS, 272, 885, arXiv:astro-ph/9406009
- Fry J. N., 1984, ApJ, 279, 499
- Heavens A., 2003, MNRAS, 343, 1327
- Garcia-Bellido J., Haugboelle T., 2008, JCAP, 0804, 003, arXiv:0802.1523
- Garcia-Bellido J., Haugboelle T., 2009, JCAP, 0909, 028, arXiv:0810.4939
- Gaztanaga E., et al., 2011, arXiv:1109.4852
- Goroff M., Grinstein B., Rey S. -J., Wise M., 1986, ApJ, 311, 6
- Goobar A., Hannestad S., Mörtsell E., Tu H., 2006, JCAP, 6, 19, arXiv:astro-ph/0602155
- Guillet T., Teyssier R., Colombi S., 2010, MNRAS, 405, 525, arXiv:0905.2615

- Guzzo L., et al., 2008, *Nature*, 451, 541-545
- Heavens A., Taylor A., 1995, *MNRAS*, 275, 483, arXiv:astro-ph/9409027
- Heavens A., 2003, *MNRAS*, 343, 1327-1334, arXiv:astro-ph/0304151
- Hirata C., 2009, *MNRAS*, 399, 1074, arXiv:0903.4929
- Hivon E., Bouchet F. R., Colombi S., Juszkiewicz R., 1995, *A & A*, 298, 643-660
- Hivon E., Górski K. M., Netterfield C. B., Brill B. P., Prunet S., Hansen F., 2002, *APJ*, 567, 2, arXiv:astro-ph/0105302
- Huchra J. P., et al., 2011, arXiv:1108.0669
- Jackson J. C., 1972, *MNRAS*, 156, 1P
- Jain B., Bertschinger E., 1994, *ApJ*, 431, 495-505, arXiv:astro-ph/9311070
- Jeong D., Komatsu E., 2006, *ApJ*, 651, 619-626, arXiv:astro-ph/0604075
- Jeong D., Komatsu E., 2009, *ApJ*, 691, 569, arXiv:0805.2632
- Juszkiewicz R., Hellwing W.A., van de Weygaert R., 2012, arXiv:1205.6163v1
- Kaiser N., 1987, *MNRAS*, 227, 1
- Komatsu E., et al., *ApJS*, 192, 18, arXiv:1001.4538
- Lanusse F., Rassat A., Starck J.-L., 2012, *A&A*, 540, A92, arXiv:1112.0561
- Laureijs R., et al., 2011, arXiv:1110.3193
- Lazkoz R., Maartens R., Majerotto E., 2006, *PRD*, 74, 083510, arXiv:astro-ph/0605701
- Leistedt B., Rassat A., Refregier A., Strack J. -L., 2011, arXiv:1111.3591
- Linder E. V., 2005, *PRD*, 72, 043529
- Makino N., Sasaki M., Suto Y., 1992, *PRD*, 68, 46, 585
- Matsubara T., 2008, *PRD*, 77, 063530
- Matsubara T., 2008, *PRD*, 78, 083519
- Matsubara T., 2011, *PRD*, 83, 083518
- Nishimichi T., et al., 2007, *PASJ*, 59, 1049, arXiv:0705.1589
- Nishimichi T., et al., 2009, *Publ. Astron. Soc. Jpn.*, 61, 321, arXiv:0810.0813
- Nock K., Percival W. J., Ross A. J., 2010, *MNRAS*, 407, 520, arXiv:1003.0896
- Nomura H., Yamamoto K., Nishimichi T., 2008, *JCAP*, 0810, 031, arXiv:0809.4538
- Nomura H., Yamamoto K., Huetsi G., Nishimichi T., 2009, *PRD*, 79, 063512, arXiv:0903.1883
- Okumura T., Jing Y. P., 2011, *APJ*, 726, 5
- Okamura T., Taruya A., Matsubara T., 2011, *JCAP*, 1108, 012
- Padmanabhan N., et al., 2005, *MNRAS*, 359, 237, arXiv:astro-ph/0407594
- Padmanabhan N., White M., Cohn J. D., 2009, *PRD*, 79, 063523, arXiv:0812.2905
- Peebles P. J. E., Yu J. T., 1970, *APJ*, 162, 815
- Percival W. J., Burkey D., Heavens A., et al., 2004, *MNRAS*, 353, 1201, arXiv:astro-ph/0406513
- Percival W. J., Cole S., Eisenstein D. J., Nichol R.C., Peacock J. A., Pope A. C., Szalay A. S., 2007, *MNRAS*, 381, 1053, arXiv:0705.3323
- Percival W. J., et al., 2007, *ApJ*, 657, 51, arXiv:astro-ph/0608635
- Rassat A., et al., 2008, arXiv:0810.0003v1 [astro-ph]
- Rassat A., Refregier A., 2012, arXiv:1112.3100
- Ross A. J., Percival W. J., Crocce M., Cabr A., Gaztanaga E., 2011, *MNRAS*, 415, 3, 2193-2204, arXiv:1102.0968
- Samushia L., et al., 2011, *MNRAS*, 410, 1993-2002
- Sato M., Matsubara T., 2011, *PRD*, 84, 043501
- Seo H. -J., Eisenstein D. J., 2003, *ApJ*, 598, 720, arXiv:astro-ph/0307460
- Seo H. -J., Eisenstein D. J., 2007, *ApJ*, 665, 14, arXiv:astro-ph/0701079
- Scoccimarro R., Frieman J., 1996, *ApJ*, 473, 620, astro-ph/9602070, arXiv:astro-ph/9602070
- Scoccimarro R., Couchman H. M. P., Frieman J. A., 1999, *ApJ*, 517, 531
- Scoccimarro R., 2004, *PRD*, 70, 083007
- Shapiro C., Crittenden R. G., Percival W. J., 2011, *MNRAS*, 422, 2341-2350, arXiv:1109.1981
- Shaw J. R., Lewis A., 2008, *PRD*, 78, 103512, arXiv:0808.1724
- Smith R. E., Scoccimarro R., Sheth R. K., 2008, *PRD*, 77, 043525, arXiv:astro-ph/0703620
- Slosar A., Ho S., White M., Louis T., 2009, *JCAP*, 10, 19, arXiv:0906.2414
- Sunyaev R. A., Zeldovich Y. B., 1970, *apss*, 7, 3
- Suto Y., Sasaki M., 1991, *PRL*, 66, 264
- Taruya A., Nishimichi T., Saito S., Hiramatsu T., 2009, *PRD*, 80, 123503, arXiv:0906.0507
- Taruya A., Nishimichi T., Saito S., 2010, *PRD*, 82, 063522, arXiv:1006.0699
- de la Torre S., Guzzo L., 2012, *MNRAS*, 427, 327-342
- Umeh O., Clarkson C., Maartens R., 2012, arXiv:1207.2109, arXiv:1207.2109
- Vishniac E., 1983, *MNRAS*, 203, 345
- Wang Y., Mukherjee P., 2006, *APJ*, 650, 1, arXiv:astro-ph/0604051
- Wang L., Steinhardt P. J., 1998, *APJ*, 508, 483
- Xu X., et al., 2010, *ApJ*, 718, 1224, arXiv:1001.2324
- York D. G., et al., 2000, *AJ*, 120, 1579, arXiv:astro-ph/0006396
- Yoo J., Desjacques V., 2013, arXiv:1301.4501
- Zaldarriaga M., Seljak U., Bertschinger E., 1998, *APJ*, 494, 491
- Zaroubi S., Hoffman Y., 1996, *APJ*, 462, 25

APPENDIX A: SPHERICAL BESSEL FUNCTION

In this section we quickly outline some of the more useful properties of the spherical Bessel functions that have been used in the derivation of our results. The first important property of spherical Bessel functions is that they obey a well-known orthogonality condition:

$$\int_0^\infty r^2 dr j_\ell(kr) j_\ell(k'r) = \frac{\pi}{2kk'} \delta(k - k'). \quad (\text{A1})$$

The first derivative of the spherical Bessel function can be expressed using the following recursion relation:

$$j'_\ell(r) = \frac{1}{2\ell + 1} \left[\ell j_{\ell-1}(r) - (\ell + 1) j_{\ell+1}(r) \right]. \quad (\text{A2})$$

The second- and higher-order derivatives are deduced by successive application of the above expression:

$$j_\ell''(r) = \left[\frac{(2\ell^2 + 2\ell - 1)}{(2\ell + 3)(2\ell + 1)} j_\ell(r) - \frac{\ell(\ell - 1)}{(2\ell - 1)(2\ell + 1)} j_{\ell-2}(r) - \frac{(\ell + 1)(\ell + 2)}{(2\ell + 1)(2\ell + 3)} j_{\ell+2}(r) \right] \quad (\text{A3})$$

These expressions can be used to simplify the kernels $I_\ell^{(1)}(k, k')$ defined in Eqn.(31) to express mode-mixing due to redshift-space distortion.

APPENDIX B: SPHERICAL HARMONICS

The spherical-harmonics are complete and orthogonal on the surface of the sphere:

$$\sum_{\ell m} Y_{\ell m}(\hat{\Omega}) Y_{\ell m}(\hat{\Omega}') = \delta^{2D}(\hat{\Omega} - \hat{\Omega}'); \quad (\text{B1})$$

$$\int d\hat{\Omega} Y_{\ell m}(\hat{\Omega}) Y_{\ell' m'}(\hat{\Omega}') = \delta_{\ell\ell'}^K \delta_{mm'}^K. \quad (\text{B2})$$

The overlap integrals of three spherical harmonics are given by the Gaunt integral which are expressed in terms of 3j symbols (denoted by matrices below):

$$\int d\hat{\Omega} Y_{\ell_1 m_1}(\hat{\Omega}) Y_{\ell_2 m_2}(\hat{\Omega}) Y_{\ell_3 m_3}(\hat{\Omega}) = I_{\ell_1 \ell_2 \ell_3} \times \begin{pmatrix} \ell_1 & \ell_2 & \ell_3 \\ 0 & 0 & 0 \end{pmatrix} \begin{pmatrix} \ell_1 & \ell_2 & \ell_3 \\ m_1 & m_2 & m_3 \end{pmatrix}; \quad (\text{B3})$$

$$I_{\ell_1 \ell_2 \ell_3} = \sqrt{\frac{(2\ell_1 + 1)(2\ell_2 + 1)(2\ell_3 + 1)}{4\pi}}. \quad (\text{B4})$$

APPENDIX C: 3J SYMBOLS

The following orthogonality properties of 3j symbols were used to simplify various expressions:

$$\sum_{\ell_3 m_3} (2\ell_3 + 1) \begin{pmatrix} \ell_1 & \ell_2 & \ell_3 \\ m_1 & m_2 & m_3 \end{pmatrix} \begin{pmatrix} \ell_1 & \ell_2 & \ell \\ m_1' & m_2' & m \end{pmatrix} = \delta_{m_1 m_1'}^K \delta_{m_2 m_2'}^K; \quad (\text{C1})$$

$$\sum_{m_1 m_2} \begin{pmatrix} \ell_1 & \ell_2 & \ell_3 \\ m_1 & m_2 & m_3 \end{pmatrix} \begin{pmatrix} \ell_1 & \ell_2 & \ell_3' \\ m_1 & m_2 & m_3' \end{pmatrix} = \frac{\delta_{\ell_3 \ell_3'}^K \delta_{m_3 m_3'}^K}{2\ell_3 + 1}. \quad (\text{C2})$$

APPENDIX D: FINITE SURVEYS AND DISCRETE SPHERICAL BESSEL-FOURIER TRANSFORMATION AND PSEUDO- C_{LS}

D1 3D Scalar fields

Different types of boundary conditions are employed in the literature for finite surveys (Binney and Quinn 1991; Fisher et al 1995; Heavens and Taylor 1995).

A natural choice for the boundary condition is to assume that the field vanishes at the boundary of the survey $r = R$ leading to following condition on the radial modes that is determined by the zeros of the spherical Bessel functions $j_\ell(r)$:

$$j_\ell(q_{\ell n}) = j_\ell(k_{\ell n} R) = 0; \quad q_{\ell n} = k_{\ell n} R. \quad (\text{D1})$$

The closure relation for spherical harmonics will take the following form:

$$\int_0^1 dz z^2 j_\ell(k_{\ell n} z) j_\ell(k_{\ell n'} z) = \frac{1}{2} [j_{\ell+1}(q_{\ell n})]^2 \delta_{\ell\ell'} \delta_{nn'}. \quad (\text{D2})$$

Which, in terms of the radial wavenumber, can be expressed as follows:

$$\int_0^R dr r^2 k_{\ell n} k_{\ell' n'} j_\ell(k_{\ell n} r) j_{\ell'}(k_{\ell' n'} r) = \frac{k_{\ell n}^2 [j_{\ell+1}(q_{\ell n})]^2}{2R^{-3}} \delta_{\ell\ell'} \delta_{nn'}. \quad (\text{D3})$$

The discrete spectrum is determined by the zeros of the spherical Bessel function. The normalisation coefficients are given by:

$$\frac{1}{\tau_{\ell n}} = \frac{R^3}{2} [k_{\ell n} j_{\ell+1}(k_{\ell n} R)]^2. \quad (\text{D4})$$

The inverse and forward discrete sFB transforms are as follows:

$$\Psi_{\ell m}(k_{\ell n}) = \tau_{\ell n} \int d^3 \mathbf{r} \Psi(\mathbf{r}) k_{\ell n} j_\ell(kr) Y_{\ell m}(\hat{\Omega}); \quad (\text{D5})$$

$$\Psi(\mathbf{r}) = \sum_{\ell m n} \tau_{\ell n} \Psi_{\ell m}(k) j_\ell(kr) Y_{\ell m}(\hat{\Omega}). \quad (\text{D6})$$

The following expression is useful:

$$\Psi_{\ell m}(k_{\ell n}) = \frac{i^\ell k_{\ell n}}{(2\pi)^{3/2}} \int d\hat{\Omega}_k \Psi(k_{\ell n}, \hat{\Omega}_k) Y_{\ell m}(\hat{\Omega}_k) \quad (\text{D7})$$

In case of finite survey the 3D power-spectrum samples only discrete radial wave-numbers $k_{\ell n}$ which is defined by the survey radius R :

$$\langle \Psi_{\ell m}(k_{\ell n}) \Psi_{\ell' m'}^*(k_{\ell' n'}) \rangle = P_{\Psi} \delta_{\ell\ell'} \delta_{mm'} \delta_{nn'}. \quad (\text{D8})$$

In addition to finite survey size, surveys often have a mask $s(\hat{\Omega})$. The sFB transform of a masked field defines the convolved or *Pseudo* harmonics $\tilde{\Psi}_{\ell m}(k_{\ell n})$:

$$\tilde{\Psi}_{\ell m}(k_{\ell n}) = \sqrt{\frac{2}{\pi}} \tau_{\ell n} \int_0^R r^2 dr \int_{\hat{\Omega}} d\hat{\Omega} \times [\phi(r) s(\hat{\Omega})] \Psi(\mathbf{r}) j_\ell(k_{\ell n} r) Y_{\ell m}(\hat{\Omega}) d\hat{\Omega}. \quad (\text{D9})$$

The convolved or *Pseudo*-harmonics are expressed in terms of all-sky

harmonics $\Psi_{lm}(k_{ln})$ by the following expression:

$$\tilde{\Psi}_{\ell m}(k_{\ell n}) = \sum_{n'} \sum_{\ell' m'} \sum_{\ell'' m''} \tau_{\ell' n'} W(k_{\ell n}, k_{\ell' n'}) \Psi_{\ell m}(k_{\ell' n'}) \times s_{\ell' m''} I_{\ell \ell' \ell''} \begin{pmatrix} \ell & \ell' & \ell'' \\ m & m' & m'' \end{pmatrix}. \quad (\text{D10})$$

The kernel $W(k_{\ell n}, k_{\ell' n'})$ depends on selection function $\phi(r)$:

$$W(k_{\ell n}, k_{\ell' n'}) = \int_0^R r^2 dr \phi(r) j_\ell(k_{\ell n} r) j_\ell(k_{\ell' n'} r) \quad (\text{D11})$$

The Pseudo- \mathcal{C}_ℓ s (PCLs) constructed from the convolved harmonics are a function of power spectrum of the angular mask $\mathcal{C}_{\ell'}^x$, normalisation coefficients $\tau_{\ell n}$ and the selection function ϕ :

$$\begin{aligned} \tilde{\mathcal{C}}_\ell(k_{\ell n}) &= \langle \tilde{\Psi}_{\ell m}(k_{\ell n}) \tilde{\Psi}_{\ell m}^*(k_{\ell n}) \rangle \\ &= \sum_{n'} \sum_{\ell'} \sum_{\ell''} \tau_{\ell' n'}^2 \frac{I_{\ell \ell' \ell''}^2}{2\ell + 1} \begin{pmatrix} \ell & \ell' & \ell'' \\ 0 & 0 & 0 \end{pmatrix}^2 \\ &\quad \times W^2(k_{\ell n}, k_{\ell' n'}) \mathcal{C}_{\ell'}(k_{\ell' n'}) \mathcal{C}_{\ell''}^x. \end{aligned} \quad (\text{D12})$$

Notice that the PCLs $\tilde{\mathcal{C}}_\ell(k_{\ell n})$ are linear superposition of the power spectrum of underlying field $\mathcal{C}_\ell(k_{\ell n})$. The mixing matrix $M_{\ell n, \ell' n'}$ is given by:

$$\tilde{\mathcal{C}}_\ell(k_{\ell n}) = \sum_{\ell' n'} M_{\ell n, \ell' n'} \mathcal{C}_{\ell'}(k_{\ell' n'}); \quad (\text{D13})$$

where the mixing matrix is given by the following expression:

$$M_{\ell n, \ell' n'} = \sum_{\ell''} \tau_{\ell' n'}^2 \frac{I_{\ell \ell' \ell''}^2}{2\ell + 1} \begin{pmatrix} \ell & \ell' & \ell'' \\ 0 & 0 & 0 \end{pmatrix}^2 W^2(k_{\ell n}, k_{\ell' n'}) \mathcal{C}_{\ell''}^x. \quad (\text{D14})$$

An unbiased estimates of the 3D power spectra can be written as:

$$\mathcal{C}_\ell(k_{\ell n}) = \sum_{\ell' n'} M_{\ell n, \ell' n'}^{-1} \tilde{\mathcal{C}}_{\ell'}(k_{\ell' n'}). \quad (\text{D15})$$

This is an extension of well known results for the projected surveys (Hivon, Górski, Netterfield, Brill, Prunet and Hansen 2002). For low sky-coverage and small survey volumes the matrix $M_{\ell n, \ell' n'}$ is expected to be singular and binning of modes may be required.

A different choice of boundary condition is often employed (Fisher et al 1995):

$$j_{\ell-1}(k_{\ell n}' R) = 0; \quad (\text{D16})$$

The normalisation constants in this case are given by:

$$\frac{1}{\tau_{\ell n}} = \frac{R^3}{2} [k_{\ell n} j_\ell(k_{\ell n} R)]^2. \quad (\text{D17})$$

The expressions for the mixing matrix derived above can still be used simply replacing the normalisation coefficients $\tau_{\ell n}$.

For discrete fields such as the galaxy distribution we can use the PCL approach if we replace the continuous function $\Psi(\mathbf{r})$ with a sum of delta functions that peak at galaxy positions r_s : $\Psi(\mathbf{r}) = \sum_{s=1}^N \delta^{3D}(\mathbf{r} - \mathbf{r}_s)$; here N is the number of galaxies. The sFB for such a discrete field is given by $\Psi_{\ell m}(k) = \sum_{s=1}^N \tau_{\ell m} j_\ell(r_s k_{\ell n}) Y_{\ell m}(\hat{\Omega}_s)$. Where the radial and angular position of galaxies are denoted by $\mathbf{r}_s = (r_s, \hat{\Omega}_s) = (r_s, \theta_s, \phi_s)$

APPENDIX E: STANDARD PERTURBATION THEORY

In the formalism outlined in section 5, any statistical observable can be computed to arbitrary order. Typically we are only interested in the second order corrections to the matter power spectrum though expressions for higher-order corrections have been derived. One of the key issues regarding the inclusion is the computational costs required for these higher-order corrections in part due to the high dimensionality of the integrals, even after symmetry arguments have been taken into account. The analytic expressions for the first corrections can be analytically derived Makino, Sasaki and Suto (1992):

$$\begin{aligned} P_{13}(k) &= \frac{1}{252} \frac{k^3}{4\pi^2} \int_0^\infty dx P_{\text{lin}}(k) P_{\text{lin}}(kx) \left[\frac{12}{x^2} - 158 + 100x^2 \right. \\ &\quad \left. - 42x^4 + \frac{3}{x^2} (x^2 - 1)^3 (7x^2 + 2) \log \left| \frac{1+x}{1-x} \right| \right] \end{aligned} \quad (\text{E1})$$

$$\begin{aligned} P_{22}(k) &= \frac{1}{98} \frac{k^3}{4\pi^2} \int_0^\infty dx P_{\text{lin}}(kx) \int_{-1}^1 d\mu P_{\text{lin}}(k\sqrt{1+x^2-2x\mu}) \\ &\quad \times \frac{(3x+7\mu-10x\mu^2)^2}{(1+x^2-2x\mu)^2} \end{aligned} \quad (\text{E2})$$

$$\begin{aligned} P_{13}^{\text{LPT}}(k) &= \frac{1}{252} \frac{k^3}{4\pi^2} P_{\text{lin}}(k) \int_0^\infty dx P_{\text{lin}}(kx) \left[\frac{12}{x^2} + 10 + 100x^2 \right. \\ &\quad \left. - 42x^4 + \frac{3}{x^3} (x^2 - 1)^3 (7x^2 + 2) \log \left| \frac{1+x}{1-x} \right| \right]. \end{aligned} \quad (\text{E3})$$

APPENDIX F: FLAT SKY LIMIT

For surveys that cover large opening angles on the sky, the full sFB expansion detailed above is the most natural and convenient choice. This expansion does, however, break down for small-angle surveys where the signal of interest occurs at high- ℓ modes. In such a situation the accurate computation of high- ℓ spherical harmonics is cumbersome and computationally expensive. Instead it is much more natural to approximate the spherical harmonics as sums of exponentials corresponding to a 2D Fourier expansion. Essentially we are replacing the spherical harmonics solutions with a plane-wave approximation valid at high multipoles.

In the flat sky limit we expand a 3D field Ψ at a 3D position $\mathbf{r} \equiv (r, \vec{\theta})$ on the sky using a basis consisting of 2D Fourier modes and radial Bessel functions:

$$f(r, \vec{\theta}) = \sqrt{\frac{2}{\pi}} \int k dk \int \frac{d^2 \vec{\ell}}{(2\pi)^2} f(k, \vec{\ell}) j_\ell(kr) e^{i\vec{\ell} \cdot \vec{\theta}} \quad (\text{F1})$$

$$f(k, \vec{\ell}) = \sqrt{\frac{2}{\pi}} \int r^2 dr \int d^2 \theta f(r, \vec{\theta}) k j_\ell(kr) e^{-i\vec{\ell} \cdot \vec{\theta}} \quad (\text{F2})$$

where ℓ is a 2D angular wavenumber and k is a conventional radial wavenumber. We can simplify the analysis by adopting coordinates such that the survey corresponds to small angles around the pole of the spherical coordinates, defined by angles (θ, ϕ) for which, in the limit $\theta \rightarrow 0$, we can apply a 2D expansion of the plane waves:

$$e^{i\vec{\ell}\cdot\vec{\theta}} \simeq \sqrt{\frac{2\pi}{\ell}} \sum_m i^m Y_{\ell m}(\theta, \phi) e^{-im\varphi_\ell} \quad (\text{F3})$$

where $\vec{\ell} = (\ell \cos \varphi_\ell, \ell \sin \varphi_\ell)$ and $\vec{\theta} = (\theta \cos \varphi, \theta \sin \varphi)$. The correspondence between the 3D flat-sky and 3D full-sky coefficients can be obtained by substituting Eq.(F3) into Eq.(F1) and noting that $\int d^2\vec{\ell} = \int \ell d\ell \int d\varphi_\ell \rightarrow \sum_\ell \ell \int d\varphi_\ell$ in the high- ℓ limit. The correspondence can be shown to be:

$$f_{\ell m}(k) = \sqrt{\frac{\ell}{2\pi}} i^m \int \frac{d\varphi_\ell}{(2\pi)} e^{-im\varphi_\ell} f(k, \vec{\ell}) \quad (\text{F4})$$

$$f(k, \vec{\ell}) = \sqrt{\frac{2\pi}{\ell}} \sum_m i^{-m} f_{\ell m}(k) e^{im\varphi_\ell} \quad (\text{F5})$$

We now extend this analysis to RSD by constructing harmonics of a field $\Psi(\mathbf{r})$ in the flat-sky limit when convolved with a selection function $\phi(s)$. These new flat-sky harmonics take into account the RSD much as before:

$$\tilde{\Psi}(k, \vec{\ell}) = \sqrt{\frac{2}{\pi}} \int s^2 ds \int d^2\theta k \Psi(r, \vec{\theta}) [\phi(s) j_\ell(ks)] e^{-i\vec{\ell}\cdot\vec{\theta}}. \quad (\text{F6})$$

Following the same perturbative procedure results in a series expansion in β where:

$$\tilde{\Psi}_\ell(k, \vec{\ell}) = \tilde{\Psi}_\ell^{(0)}(k, \vec{\ell}) + \tilde{\Psi}_\ell^{(1)}(k, \vec{\ell}) + \dots \quad (\text{F7})$$

As before the $\tilde{\Psi}_\ell^{(0)}(k, \vec{\ell})$ term represents the unredshifted contribution:

$$\tilde{\Psi}_\ell^{(0)}(k, \vec{\ell}) = \sqrt{\frac{2}{\pi}} \int r^2 dr \int d^2\theta \Psi(r, \vec{\theta}) k [j_\ell(kr) \phi(r)] e^{-i\vec{\ell}\cdot\vec{\theta}} \quad (\text{F8})$$

$$\begin{aligned} \tilde{\Psi}_\ell^{(1)}(k, \vec{\ell}) &= \sqrt{\frac{2}{\pi}} \int r^2 dr \int d^2\theta \Psi(r, \vec{\theta}) k \\ &\times \left\{ [\mathbf{v}(\vec{r}) \cdot \vec{\theta}] \frac{d}{dr} [j_\ell(kr) \psi(r)] \right\} e^{-i\vec{\ell}\cdot\vec{\theta}} \end{aligned} \quad (\text{F9})$$

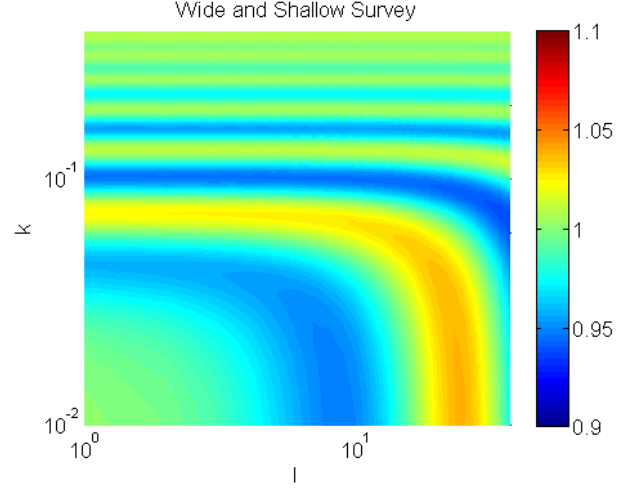


Figure 4. Ratio $R_\ell^C(k)$ of sFB spectrum with and without the physical effects of baryons in (ℓ, k) phase space for a wide and shallow survey of $r_0 = 100h^{-1}\text{Mpc}$ using a Gaussian selection function. The baryonic wiggles are seen in both the radial (k) and tangential (ℓ) directions.

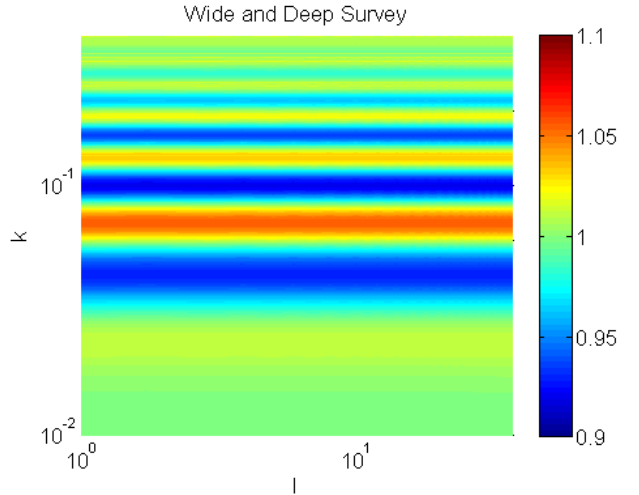


Figure 5. Ratio $R_\ell^C(k)$ of sFB spectrum with and without the physical effects of baryons in (ℓ, k) phase space for a wide and deep survey of $r_0 = 1400h^{-1}\text{Mpc}$ using a Gaussian selection function. The baryonic wiggles are seen in both the radial (k) and tangential (ℓ) directions.

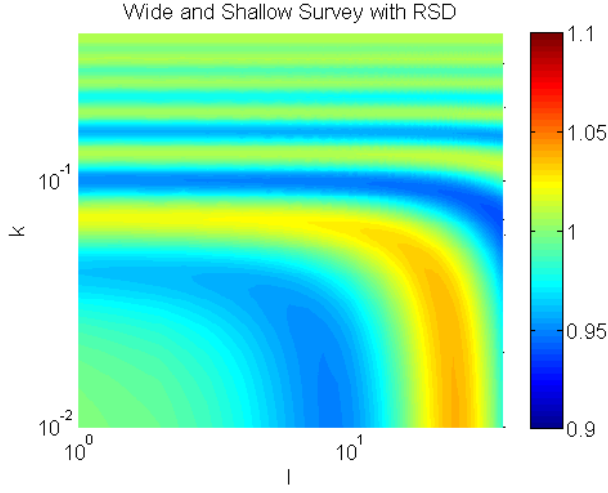


Figure 6. Ratio $R_\ell^C(k)$ of sFB spectrum with and without the physical effects of baryons in (ℓ, k) phase space for a wide and shallow survey of $r_0 = 100h^{-1}\text{Mpc}$ using a Gaussian selection function but with the inclusion of redshift space distortions.

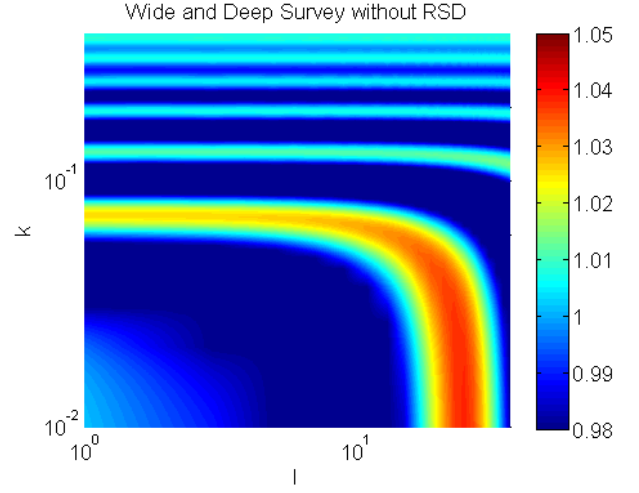


Figure 8. Ratio $R_\ell^C(k)$ of sFB spectrum for a wide and shallow survey of $r_0 = 100h^{-1}\text{Mpc}$ using a Gaussian selection function without RSD. Here we have reduced the dynamic range to highlight the impact that RSD have on the BAOs. This plot is equivalent to Figure [4]. Compare to Figure [9] to see the phenomenological effects of RSD.

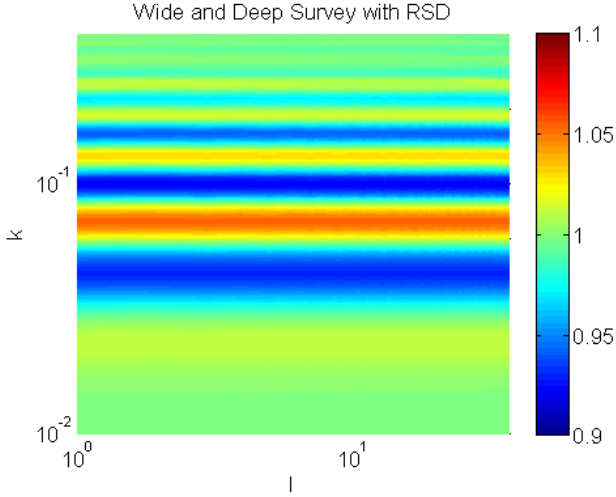


Figure 7. Ratio $R_\ell^C(k)$ of sFB spectrum with and without the physical effects of baryons in (ℓ, k) phase space for a wide and deep survey of $r_0 = 1400h^{-1}\text{Mpc}$ using a Gaussian selection function but with the inclusion of redshift space distortions.

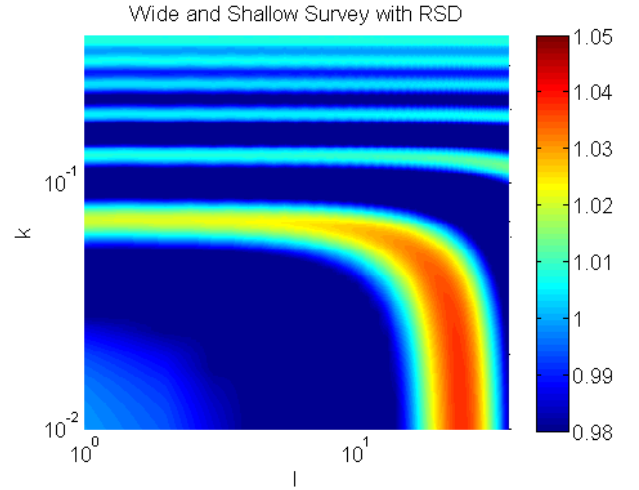


Figure 9. Ratio $R_\ell^C(k)$ of sFB spectrum for a wide and shallow survey of $r_0 = 100h^{-1}\text{Mpc}$ using a Gaussian selection function but with the inclusion of RSD. Here we have reduced the dynamic range to highlight the impact that RSD have on the BAOs. This plot is equivalent to Figure [6]. Compare to the unredshifted results of Figure [8]. RSD suppress the power at lower ℓ and k modes and smear the wiggles in the k direction. Power in the first peak is reduced as per Figure 1 but the amplitudes level at higher ℓ .

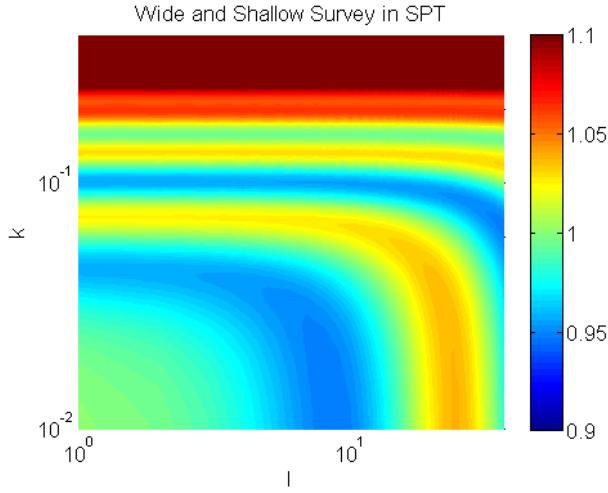


Figure 10. Ratio $R_\ell^C(k)$ of sFB spectrum with and without the physical effects of baryons in (ℓ, k) phase space for a wide and shallow survey of $r_0 = 100h^{-1}\text{Mpc}$ using a Gaussian selection function but with the inclusion of non-linear features as calculated in Standard Perturbation Theory.

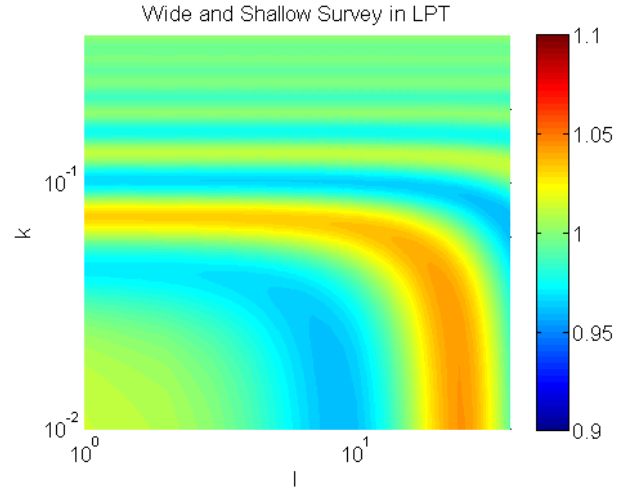


Figure 12. Ratio $R_\ell^C(k)$ of sFB spectrum with and without the physical effects of baryons in (ℓ, k) phase space for a wide and shallow survey of $r_0 = 100h^{-1}\text{Mpc}$ using a Gaussian selection function but with the inclusion of non-linear features as calculated in LPT.

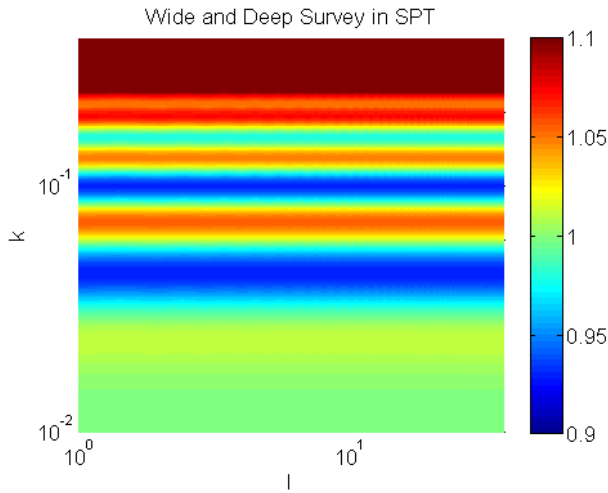


Figure 11. Ratio $R_\ell^C(k)$ of sFB spectrum with and without the physical effects of baryons in (ℓ, k) phase space for a wide and deep survey of $r_0 = 1400h^{-1}\text{Mpc}$ using a Gaussian selection function but with the inclusion of non-linear features as calculated in Standard Perturbation Theory.

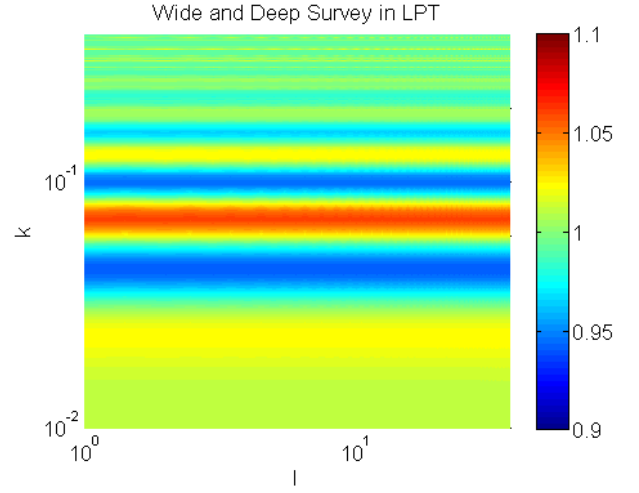


Figure 13. Ratio $R_\ell^C(k)$ of sFB spectrum with and without the physical effects of baryons in (ℓ, k) phase space for a wide and deep survey of $r_0 = 1400h^{-1}\text{Mpc}$ using a Gaussian selection function but with the inclusion of non-linear features as calculated in LPT.